The Thesis Committee for José Santiago Enriquez
Certifies that this is the approved version of the following thesis:

Cysteine Responsive Copper(II) Based ^{19}F MRI Probes

APPROVED BY
SUPERVISING COMMITTEE:

Supervisor:

Emily Que

Michael J. Rose

Cysteine Responsive Copper(II) Based ^{19}F MRI Probes

by

José Santiago Enriquez

Thesis

Presented to the Faculty of the Graduate School of

The University of Texas at Austin

in Partial Fulfillment

of the Requirements

for the Degree of

Master of Arts

The University of Texas at Austin

December 2017

Acknowledgements

I would like to thank everyone in the Que lab that have supported and motivated me through grad school. Especially Dr. Meng Yu, Da Xie, Radhika Mehta, Rahul Kadakia, Chinh Ngo, Bailey Bouley and many others. My two summer high school students, Sonya Xu and Daniel Han, who helped with the synthesis of various ligands and complexes. Also, I want to thank my family for always being there for me and supporting me whatever the situation might be.

Abstract

Cysteine Responsive Copper(II) Based ^{19}F MRI Probes

José Santiago Enriquez, M.A.

The University of Texas at Austin, 2017

Supervisor: Emily Que

Cysteine plays an important role upholding cellular homeostasis by maintaining a proper redox environment. Perturbations in cysteine concentration may lead to cardiovascular and liver disease, and cancer, making cysteine an important amino acid to detect and monitor. In order to detect cysteine *in vitro* and *in vivo* it is advantageous to choose an imaging tool with high tissue penetration, low background noise, and less radiation, which led us to ^{19}F MRI. Herein we report a series of copper complexes with fluorine moieties appended to the macrocycle cyclam for use of ^{19}F MRI detection of cysteine. In this study, an efficient "turn-on" response was observed upon reduction of the Cu(II) complexes by cysteine. This response was characterized using UV/Vis absorption spectroscopy, NMR, EPR, and ^{19}F MRI. Early biological results suggest that these probes can detect cysteine in red blood cells, opening the doors for further animal studies.

Table of Contents

I. Introduction

Cysteine is an essential amino acid in the body that plays an important role in the regulation of many cellular processes, including maintaining the redox homeostasis in cellular environments.[1, 2] Cysteine is also involved as the building block in the synthesis of glutathione (GSH)[3], an important tripeptide that is an abundant intracellular redox buffer, and it is a well-known bio-reductant alongside GSH, NADH, and HNO.[4] The intracellular concentration of cysteine varies from 30 to 200 μM depending on the cell type. Perturbations in the concentration of cysteine are associated with diseases such as cardiovascular diseases, liver disease, and cancer.[5, 6]

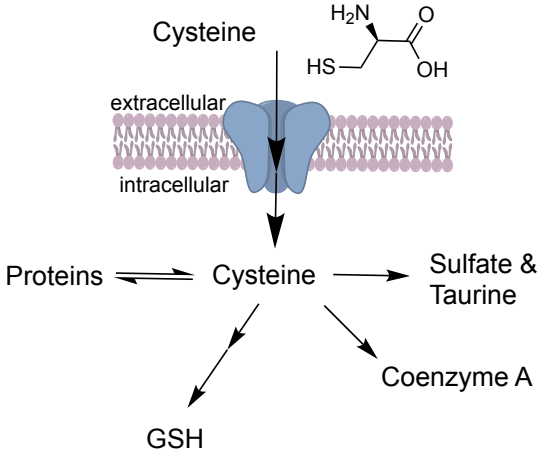

Figure 1. Cysteine pathway into the cell and its metabolism. Adapted from reference 4

The important role of cysteine in both health and disease has led to the development of probes to detect and monitor its intracellular levels.[7] Most of these probes rely on fluorescence turn-on to track cysteine at the cellular level by either a structural or activity change.[8, 9] However, translating these studies into animal models is limited by the poor penetration depth of fluorescence microscopy. [9, 10]

In our study, we propose one of the first probes to track cysteine using Magnetic

Resonance Imaging (MRI) a non-invasive diagnostic imaging modality with high penetration depth.[11] Currently, clinical MRI images protons (^{1}H) in the body, but due to the large amounts of water, these images include a significant amount of background signal. A suitable alternative is ^{19}F MRI, due to the negligible amount of fluorine in the body, the 100% percent abundance of ^{19}F, and its similar characteristics to ^{1}H. Which include a similar gyromanetic ratio, a nuclear spin of ½, and a comparable sensitivity: 83% relative to that of proton.[12]

The ability to have an enhanced signal or a turn on-off switch is essential in ^{1}H MRI as well as ^{19}F MRI. To achieve this, scaffolds are developed with metals such as lanthanides,[13] which are chosen due to their highly paramagnetic nature. There have been multiple reports of ^{19}F-based MR sensors, some of them including a Gd^{3+} center with seven unpaired electrons, that acts as the turn "off" switch. In one example, a fluorine moiety is linked to the Gd^{3+} center by a peptide sequence. After incubation with specific proteases, the peptide is cleaved and a turn–on in signal is observed.[14, 15] This strategy is also seen with the detection of β-galactosidase.[16] Another example involves using a fluorine filled nanoparticle that has gadolinium complexes bound by a disulfide bond. The bound gadolinium complexes act as the 'quencher' of the system. After cleavage of the disulfide bond by a reductant, a turn "on" in fluorine signal is observed due to the dissociation of the Gd complexes.[17]

In the Que lab, we make use of the paramagnetic effect on ^{19}F signals by employing the first row transition metals. One example is cobalt, which can be used to detect biological oxidants. Cobalt(II) oxidizes to cobalt(III) by cellular oxidants and this results in a change from a high spin paramagnetic state to a low spin diamagnetic state.[18] Other groups have used other first row transition metals including Ni[19], Mn[20],

Fe[21] and Cu for modulating ^{19}F signal.[22]

In our case, we have selected Cu(II) for our sensor probes due to its ability to be reduced by bioreductants.[23] Copper is also a straightforward system to use as it generally exists in one of two possible oxidation states. Each oxidation state has different properties, Cu(II) is paramagnetic as it contains an unpaired electron, while Cu(I) is diamagnetic. Since a one electron transfer is needed to reduce Cu(II) to Cu(I), this makes it suitable to detect reducing environments. This effect can be studied using ^{19}F NMR and MRI, as the paramagnetic Cu(II) will "quench" the fluorine signal via paramagnetic relaxation enhancement (PRE). The long electronic relaxation time of Cu(II) results in drastic reduction in T_1/T_2 relaxation times and severe line broadening, effectively quenching the ^{19}F signal. Once the copper is reduced to Cu(I), the signal will reappear as the PRE disappears and short T_{1e} of Cu(I) giving the turn "on" in the system.[22, 24] With the introduction of copper into a biological setting with high concentration of bioreductants, this redox event can occur given appropriate ligand design and can be tracked by ^{19}F magnetic resonance (NMR or MRI).

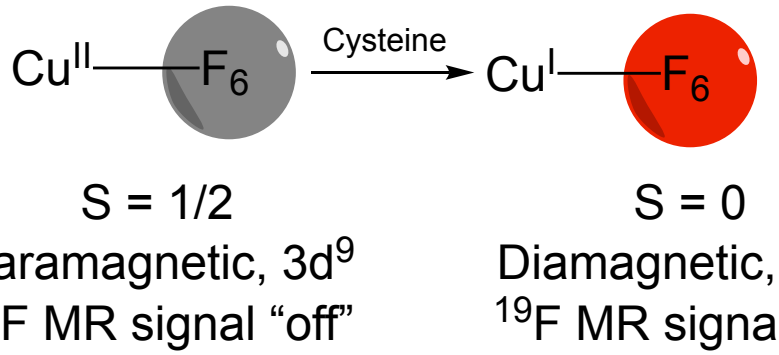

Scheme 1. Copper going from paramagnetic to diamagnetic system and its effects on MR signal

The key to designing a cysteine-responsive ^{19}F MRI probe is tuning the potential

of the Cu(II)/Cu(I) redox couple. Another important requirement is the presence of a strong and flexible metal chelator to prevent metal disassociation. Additionally, water solubility is key for biocompatibility. Cyclam was chosen as a favorable ligand scaffold owing to its high binding affinity towards Cu(II) ($pK_d \approx 25$).[25] Addition of aromatic or alkyl substituents on the macrocyclic ring can shift the $E_{1/2}$ of Cu(II)/Cu(I) cathodically which renders the Cu(II) complex more prone to reduction by weaker reductants like cysteine: an idea that has been demonstrated by some reported NO or HNO fluorescence sensors.[26] Based on this strategy, four different ligands and their corresponding Cu(II) complexes were synthesized. (Scheme 2) The first two ligands have a benzyl appended to the macrocycle, with a CF_3 group in the *ortho*- position. The first ligand has just one benzyl and the second has two benzyls with CF_3 groups appended on opposite sides of the macrocycle. To increase water solubility in the system, the benzyl moiety was replaced by a methylene linker, inspired by a report from Kotek and co-workers who recently reported water-soluble nickel cyclam analogues.[15] Two ligands were designed with this in mind, one with only one methylene linker and the other with two on opposite sides of the macrocycle, as seen in Scheme 2 for **3** and **4**.

Here we report smart ^{19}F MRI probes with the ability to detect bioreductants, specifically cysteine. With an accessible synthetic path and an efficient “off-on” response with only three equivalents of cysteine, an improvement from previous cysteine probes. Response of these probes to cysteine in buffer and mixed organic/buffer solutions are described and cell experiments are currently ongoing.

II. Results and Discussion

The ligand Cyclam$BnCF_3$ (**1b**) was readily synthesized in 60% yield by a one-step reaction between cyclam and 2-trifluoromethylbenzyl bromide. Di-substituted Cyclam$(BnCF_3)_2$ (**2c**) was obtained by reaction between bisformyl cyclam and two equivalents of 2-trifluoromethylbenzyl bromide, followed by base-mediated hydrolysis to yield the desired product in 40% overall yield over three steps (Synthesis for 2. Compound 2b). The ligand Cyclam$(CH_2CF_3)_2$ (**4d**) was successfully synthesized using a modified literature procedure.[27] The ligand CyclamCH_2CF_3 (**3d**), was synthesized by protecting the cyclam with benzyl bromide to form the tris alkylated species and reacting with trifluoro-acetic anhydride. Then a double reduction was performed, the carbonyl to a methylene followed by a benzyl reduction yielded the final ligand. The copper complexes **1**, **2**, **3**, and **4** were produced by combining ligand and $Cu(ClO_4)_2$ in methanol, and purified by washing the precipitate with diethyl ether or by the use of reverse-phase chromatography in 70%, 80%, 40%, and 80% yield, respectively.

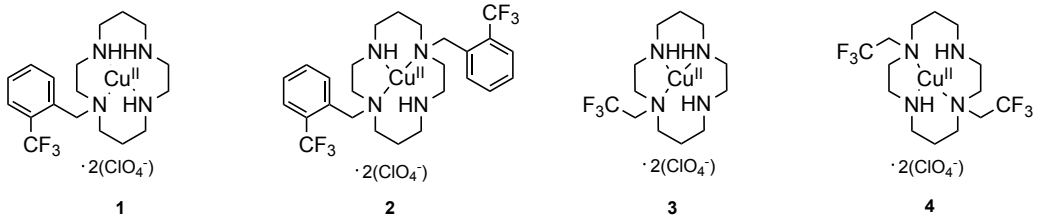

Scheme 2. Copper complexes synthesized in this study

Single crystals suitable for X-ray diffraction were obtained by slow evaporation of CH_3CN/H_2O (3:7) solutions of **1**, **2**, and **4**. (Figure 2) All crystal structures reveal distorted octahedral geometry with four nitrogen atoms occupying the equatorial plane and two oxygen atoms from perchlorate ions in the axial positions. All three structures

possess a *trans*-III configuration in the solid state with two adjacent N-R groups of the macrocycle (R = H or the alkyl group) pointing towards one side of the cyclam plane while the other two pointing to the opposite side. As expected, the introduction of trifluorobenzyl or trifluoromethyl groups on the nitrogen atoms results in substantial Cu-N bond elongation (0.1 Å) compared to the other Cu-N bonds which is likely due to a combination of steric and electron-withdrawing effects. The Cu-F average distances were determined to be 5.63, 5.69, and 5.60 Å for complex **1**, **2**, and **4**, respectively, well within the range for the PRE effect.[28] For complex **3,** crystals were obtained but were not suitable for X-ray diffraction.

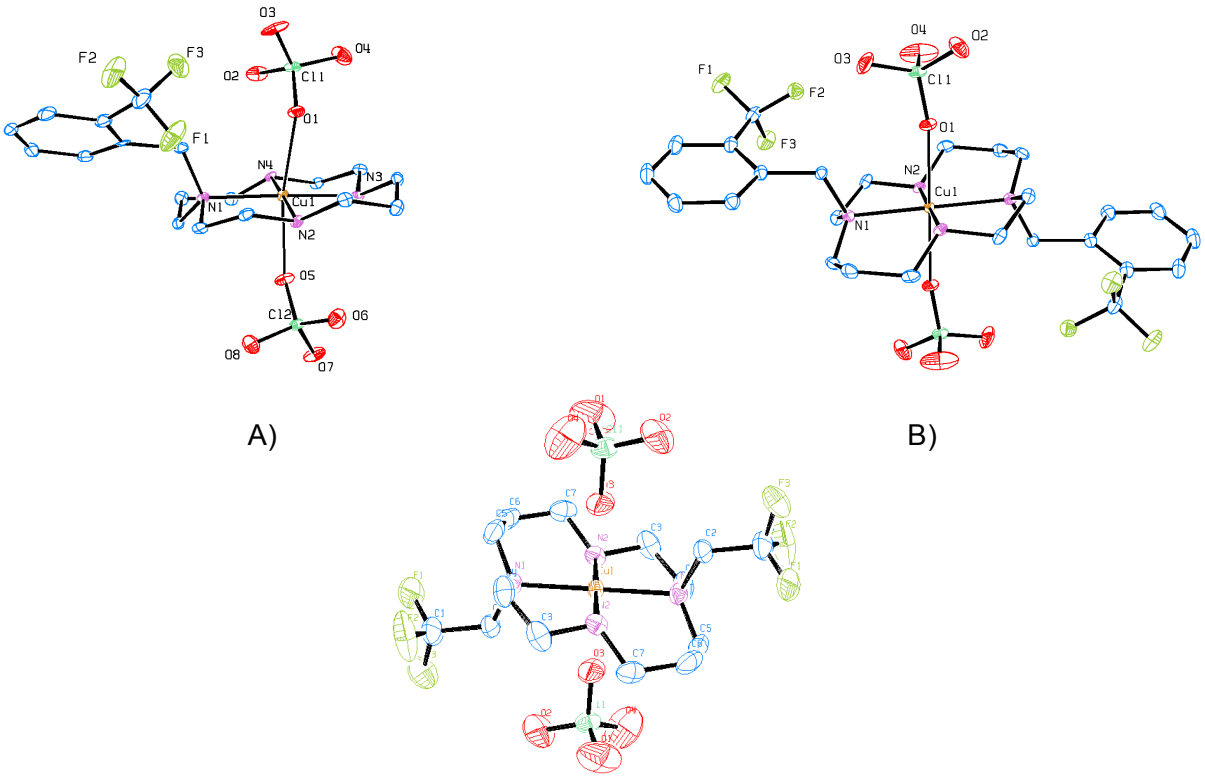

Figure 2. A) ORTEP drawing of *trans*-III $[Cu(CyclamBnF_3)](ClO_4)_2$ (**1**), B) *trans*-III $[Cu(CyclamBnF_6)](ClO_4)_2$ (**2**); C) *trans*-III $[Cu(CyclamCF_6)](ClO_4)_2$ (**4**); the thermal ellipsoids are at the 50% probability level.

Complexes **1** and **2** exhibited water solubility limitations as an organic co-solvent was needed to dissolve these complexes in aqueous solutions. The best ratio was found to be 6:4 HEPES/CH_3CN. This is likely due to the hydrophobic benzyl rings appended to the cyclam moiety. As for complexes **3** and **4,** the water solubility was greatly improved. Complex **3** is soluble up to 5mM in either water or HEPES buffer and **4** is soluble up to 1mM in water and HEPES buffer.

The UV-vis spectrum of **1** displays a distinct d-d transition band at 530 nm (ε = 220 $M^{-1}cm^{-1}$, Figure 3) in HEPES/CH_3CN solution (HEPES: 50 mM, pH 7.2, NaCl 0.1 M; HEPES:CH_3CN = 6:4 v/v), **2** exhibits an analogous absorption feature at 563 nm (ε = 384 $M^{-1}cm^{-1}$, Figure 3). Complex **3** in HEPES buffer displays a distinct d-d transition at 537 nm (ε = 124 $M^{-1}cm^{-1}$) and for complex **4** in HEPES displays an absorption feature at 548 nm (ε = 212 $M^{-1}cm^{-1}$). These values are comparable to those reported for tetracoordinate cyclam copper(II) complexes with square-planar geometry.[29] Changing the solvent to a noncoordinating solvent (nitromethane) shifted the wavelength from 530 to 513 nm (ε = 256 $M^{-1}cm^{-1}$) and from 563 to 529 nm (ε = 303 $M^{-1}cm^{-1}$) for **1** and **2**, respectively. These relatively small shifts in absorbance are consistent with a square-planar coordination environment in solution without solvent molecules directly coordinating to the metal center after replacing the labile perchlorates.[30]

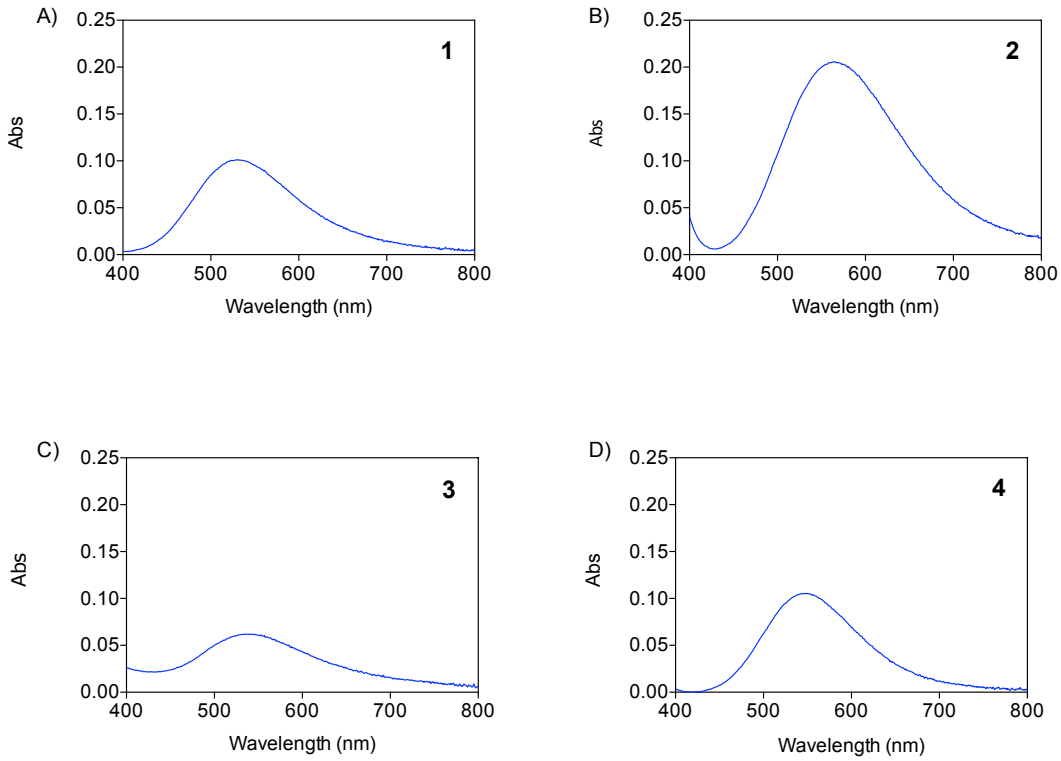

Figure 3. UV/Vis spectra of A) 0.5 mM **1** B) 0.5 mM **2** C) 0.5 mM **3** D) 0.5 mM **4**

The electrochemical properties of **1**-**4** were studied using cyclic voltammetry. In DMF solution, (Figure 4) complex **1** gave a quasi-reversible feature with $E_{1/2}$ = -1.04 V (vs ferrocene, ΔE = 226 mV) which was assigned to the Cu(I)/Cu(II) redox couple. A similar feature was observed in complex **2** with a more positive redox potential $E_{1/2}$ = –0.74 V (ΔE = 117 mV); this was comparable to a reported NO sensor with two anthracene moieties appended to the cyclam ring ($E_{1/2}$ = -0.61 V). Introduction of a second trifluoromethylbenzyl ring shifts the redox potential positively by 300 mV. This is likely due to the relief of steric strain caused by the benzyl substituents upon changing from octahedral Cu(II) to tetrahedral Cu(I) geometry. This can also be due to the change

in the donor strength as the nitrogens were substituted by a electron withdrawing group. As a control to study the effect of the electron withdrawing CF_3 group in our system, a complex without any CF_3 groups was synthesized by reacting cyclam with benzyl bromide and then $Cu(ClO_4)_2$ (**5**). The redox potential was even more negative ($E_{1/2}$ = -0.93 V), suggesting that the incorporation of a trifluromethyl group was helpful in positively shifting the redox potential of the system. In addition to the number of CF_3 groups shifting the redox potential, the position of this group was also important. A system with the CF_3 group at the *para*- position instead of the *ortho*- position, as seen in complex **1** and **2**, was obtained (**6**) and a redox potential of -0.88 V was observed. Compared to complex **2**, there was a 140 mV negative shift, most likely due to an inductive effect and position of the CF_3 group. Under the same conditions, complex **3** gives a feature at $E_{1/2}$ = -0.96 V (ΔE = 400 mV). Similarly in complex **4** a quasi-reversible feature was observed at $E_{1/2}$ = –0.74 V (ΔE = 127 mV), which were comparable with the benzyl systems. Moreover, an irreversible oxidation peak was observed in all complexes **1**-**4** with E^0 = -0.24 V, -0.38 V, -0.12 V, and -0.23 V respectively. This feature was reminiscent of the redox behavior in the Cu(II) complex of tetramethylcyclam (TMC) and has been attributed to the rapid structural reorganization or isomerization of the Cu(I) *trans*-III intermediate in the TMC system.[31]

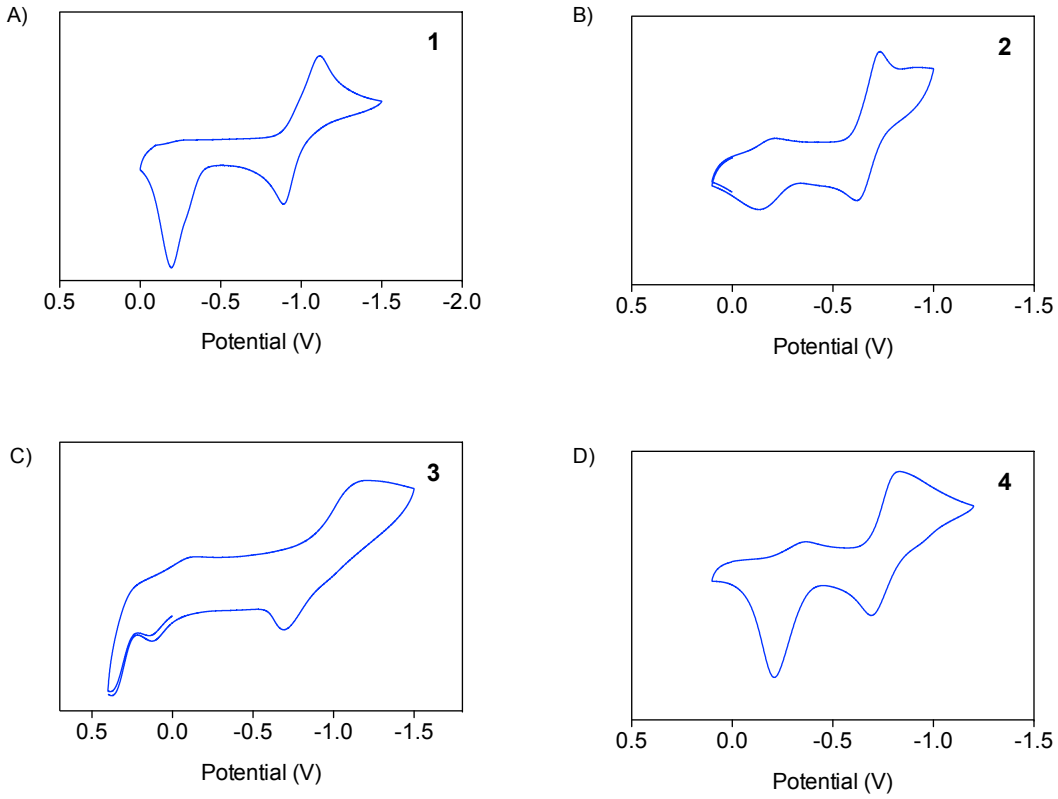

Figure 4. A) Complex **1**, B) Complex **2**, C) Complex **3**, D) Complex **4**; 1 mM in DMF, three-electrode cell; a platinum electrode as working electrode, an Ag/Ag+ non-aqueous electrode as reference and a platinum wire as auxiliary electrode. Bn_4NBF_4 (0.1 M) was used as the electrolyte and the spectra were calibrated by ferrocene.

In order to investigate the reactivity of complexes **1**-**4** towards cysteine, UV/Vis absorption spectroscopy was used to monitor the reduction process following the characteristic d-d transition band. Complexes **1** and **3** show limited reactivity towards cysteine. For complex **1**, only 43% reduction was observed in 40 min in the presence of 12 equiv. of cysteine. For complex **3** only 55% reduction was observed after 10 minutes in the presence of 9 equiv. of cysteine (Figure 5). Conversely, reaction of complexes **2** and **4** with cysteine was rapid and associated with the color change from purple to colorless (Figure 5). For complex **2**, based on the absorbance at 563 nm, about 39%

reduction was achieved upon the addition of 1 equiv. cysteine and this conversion was increased to 74% after the introduction of a second equiv. of cysteine. The reduction process was driven to almost full completion with 3 equiv. cysteine. With complex **4** a 45% reduction was achieved with 1 equiv. of cysteine, with 2 equiv. a 70% reduction was observed. Finally with 3 equiv. of cysteine, there was a complete reduction. Interestingly, the reduction of **2** and **4** appears to be reversible as the reacted solution gradually changed from colorless back to purple upon exposure to air within 30 min and 1 hr, respectively. The re-oxidation of **2** was accompanied by the reappearance of the d-d transition band at 563 nm in the UV-vis spectrum. It is noteworthy that for complex **2** only ~75% regeneration was obtained according to the absorbance assuming the original Cu(II) complex was reformed. Part of the Cu(I) complex likely underwent ligand dissociation and formed a Cu(I)-cysteine complex which has a characteristic band at 260 nm and a shoulder at 300 nm.[32] These bands were observed following the reaction of **2** and cysteine. Additionally, some white precipitate was observed during the process, which was identified to be free ligand by LC/MS and X-ray crystallography. For complex **4**, there was only ~85% regeneration, also due to ligand dissociation. Given the promising results of **2** and **4**, our following study mainly focused on these complexes.

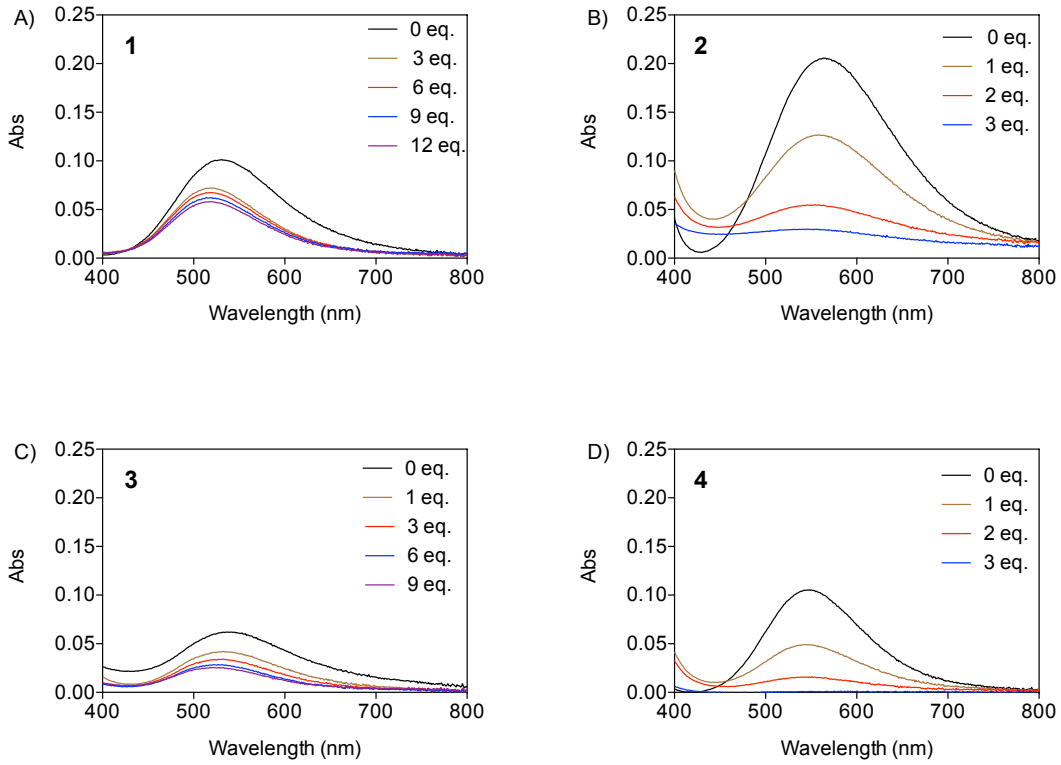

Figure 5. UV/Vis cysteine titration A) 0.5 mM **1** in O_2-free HEPES/CH_3CN (6:4) solution B) 0.5 mM **2** in O_2-free HEPES/CH_3CN (6:4) C) 0.5 mM **3** in O_2-free HEPES solution D) UV/Vis titration of 0.5 mM **4** in O_2-free HEPES solution. Spectra were scanned immediately after the addition of cysteine.

To better understand the reaction between cysteine and complexes **2** and **4**, we used EPR to monitor the presence of paramagnetic species in solution. Consistent with the crystal structure, the EPR spectra of **2** and **4** in HEPES buffer revealed square planar or octahedral geometries with elongated axial bonds ($g_z > g_x$, $g_y > g_e$).[29] After the addition of 3 equiv. cysteine, full disappearance of the EPR signals was observed in both complexes, which suggested the reduction from Cu(II) to Cu(I) instead of metal displacement by cysteine. (Figure 6) After exposing the reduced sample to air, the EPR

signal for both complexes was partially restored. Double integration of the EPR spectra revealed a 74% signal restoration for **2** and 90% signal restoration for **4**, consistent with the percent recovery observed by UV/Vis. Moreover, the EPR hyperfine features after re-oxidation perfectly matched the EPR spectra of **2** and **4**, indicating the coordination environment was maintained and confirmed the regeneration of both complexes**.**

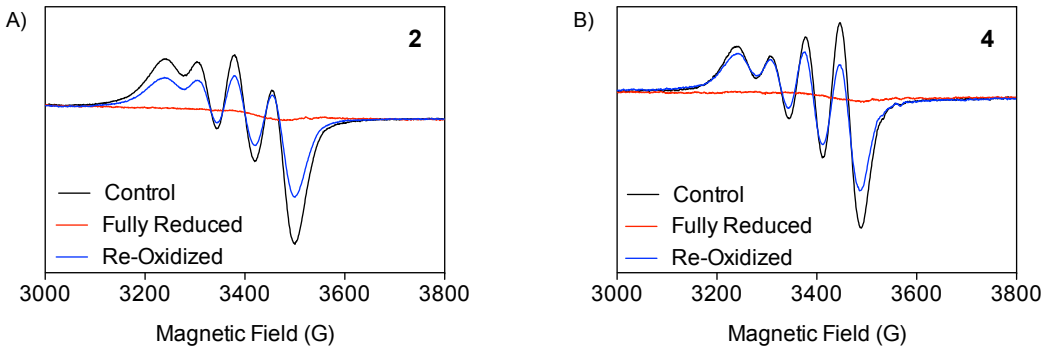

Figure 6**.** A) EPR spectra of 2 mM **2** in O_2-free HEPES/CH_3CN (6:4) solution and after treating with 3 equiv. cysteine. The reduced sample was then exposed to air for 30 min. B) EPR spectra of 2 mM **4** in O_2-free HEPES solution and after treating with 3 equiv. cysteine. The reduced sample was then exposed to air for 1 hour.

NMR spectroscopy was used to further analyze the reaction between **2** and **4** and cysteine. The ^{19}F NMR spectrum of **2** displays a severely broadened peak at -52.5 ppm. The T_1/T_2 relaxation times of ^{19}F nuclei could not be accurately determined and were estimated to be <0.1 ms. For complex **4** the ^{19}F peak was completely attenuated. This was mainly attributed to the long electronic relaxation time (T_{1e}) of Cu(II) (0.1-10 ns) and the close distance between Cu(II) and fluorine atoms in these complexes. After reacting with cysteine, in **2** a sharp singlet at -58.2 ppm appeared which was assigned to the generated Cu(I) complex. Only one single ^{19}F signal was observed upon reduction which was critical for higher sensitivity in ^{19}F MRI.[33] This is in contrast to most DOTA-

based lanthanide complexes with trifluoroaryl moieties that exhibit multiple ^{19}F signals. One plausible explanation is that the flexibility of cyclam ring increases the rate of isomerization and exceeds the NMR timescale.[34] For complex **4** a sharp triplet at -67.5 ppm was generated upon reacting with cysteine. This is consistent to the coupling between the methylene group adjacent to the CF_3 moiety. The signal intensity increased gradually as more equivalents of cysteine were introduced (Figure 7). Moreover, this signal vanished over time upon exposure to air due to re-oxidation to Cu(II). The T_1 and T_2 relaxation times of the ^{19}F signal of **2** after reduction were 1.2 s and 0.60 s, respectively, which vary from those of the ligand (1.0 s, 0.80 s). The T_1 and T_2 relaxation times of the ^{19}F signal of **4** after reduction were 2.0 s and 1.6 s, respectively.

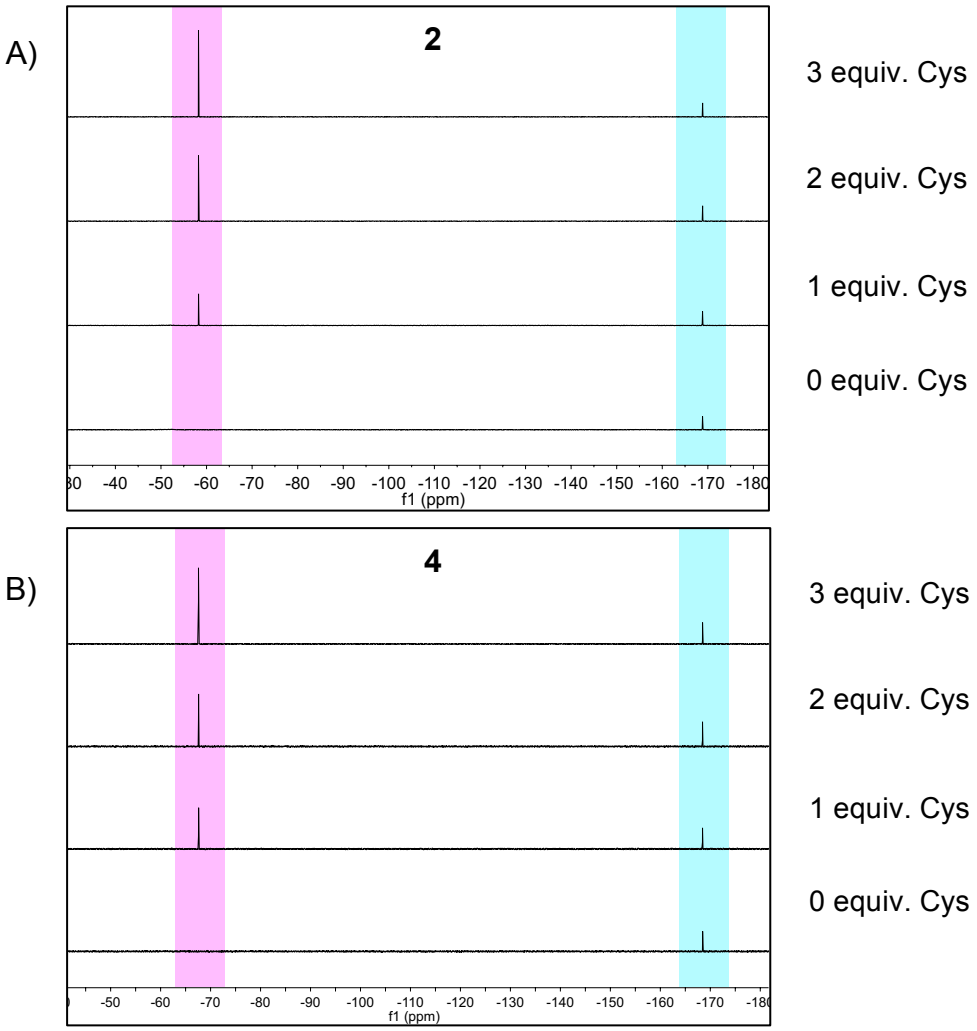

Figure 7. ^{19}F NMR spectra A) 2 mM **2** in HEPES/CH_3CN (6:4) in presence of 0 to 3 equiv. of cysteine. (bottom to top) The broad peak at -58.2 ppm was assigned to **2**; the peak at -58.2 ppm corresponds to the Cu(I) complex reduced by cysteine. B) 2 mM **4** in HEPES in the presence of 0 to 3 equiv. of cysteine. (bottom to top) The peak at -67.5 ppm corresponds to the Cu(I) complex reduced by cysteine; the peak at -168.43 ppm is 5F-cytosine as the internal standard.

We suggest the following mechanism. (Figure 8) First there is a one-electron transfer to the copper center by one of the cysteines. Like mentioned before, the reduced Cu(I) complex most likely underwent ligand disassociation. After the oxidation of one cysteine it forms a disulfide bond with another oxidized cysteine making cystine. ^1H

NMR spectra of **2** in presence of 3 equiv. cysteine exhibits well defined peaks that are distinct from the ligand which can be identified as cysteine and cystine. Features of cystine in the NMR spectra supports the one-electron transfer from cysteine to Cu(II).[35] After the formation of cystine, more equivalents of cysteine were needed to reduce all the remaining copper centers in solution. Due to the oxidizing properties of copper in aqueous solutions another equivalent of cysteine was required. This cysteine serves to stabilize the reduced copper center and maintain the copper(I) state in solution with a Cu(I)-Cys complex.[32] Evidence of the Cu(I)-Cys complex was previously mentioned with the cysteine reduction UV/Vis results.

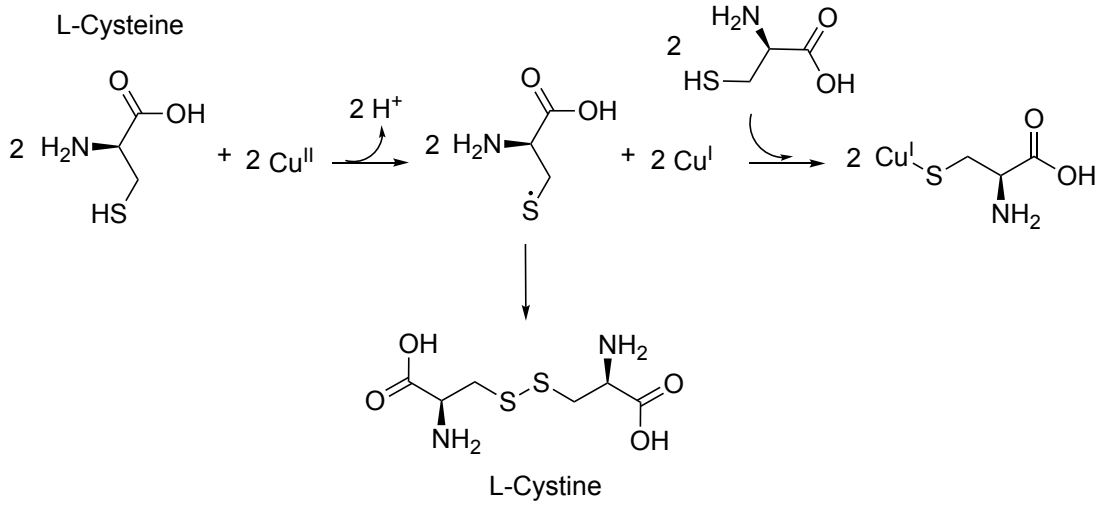

Figure 8. Proposed mechanism of reduction based on stoichiometry and reference.[32]

Selectivity of **2** and **4** towards other amino acids and reductants was further explored. The amino acids tested were, glycine, histidine, methionine, threonine, and serine, which resulted in no change based on the UV/Vis spectra, as the d-d transition did not decrease. As an abundant biological reductant, glutathione (GSH) plays an important role in maintaining cellular redox potential. However, no reaction with 5 equiv.

of glutathione was observed in UV/Vis after 1 h. We noted that slow discoloration was seen over a week, corresponding to a slow reduction. Another bio-reductant and biothiol that was tested was homocysteine, as it is structurally similar to cysteine. It was observed that there was reactivity, as partial reduction was seen with 5 equiv., but not the same degree as cysteine. Nitrogen containing species, such as NO, $NaNO_2$ and $NaNO_3$ exhibited no reactivity towards both **2** and **4** according to UV/Vis. Although excess HNO generated using Angeli's salt can induce a significant absorbance decrease in UV/Vis, EPR study revealed that the difference was probably due to metal displacement as strong, distinct EPR Cu(II) signals were still present after reacting **2** with 20 equiv. HNO. Overall, complexes **2** and **4** displayed selectivity for cysteine over biological reductants such as glutathione, homocysteine, and HNO.

The capability of **2** and **4** to detect cysteine in solution by ^{19}F MRI was explored using a 7 T MRI scanner. Three samples of each complex were prepared. First, a 4 mM of **2** was prepared in HEPES:CH_3CN mixture. Then another 4 mM of **2** in the same mixture was allowed to react with 12 mM cysteine for 30 min. The last sample of **2** consisted of a 4 mM solution that reacted with 12 mM of cysteine and then was exposed to air for 1 hour. The same three samples were prepared for **4**, but only in HEPES buffer instead of the solvent mixture. Spin-density weighted ^{19}F MRI images were acquired for the three samples using a T_1-RARE pulse sequence. As expected, complexes **2** and **4** exhibit no detectable MRI signal due to their short T_1/T_2 relaxation times as indicated by the severely broadened ^{19}F signal in NMR spectra. (Figure 9) Conversely, in complex **2** with the cysteine treated sample displayed good MRI signal with SNR of 23. After the sample was exposed to air the SNR decreased to 10, which corresponds to a re-oxidation of the complex. For complex **4** the sample treated with cysteine displayed

similar MRI signal as **2**, with a SNR of 44 and after it was let re-oxidized for 1 hour the MRI signal intensity greatly decreased to a SNR of 13 (Figure 9). The main reason contributing to the decreased signal intensity in **2** relative to **4** is related to the decomposition of the Cu(I) complex due to the strong binding affinity of cysteine towards Cu(I) as well as the unfavourable geometry of the cyclam N4 binding site for Cu(I); this generated Cu(I)-cysteine complex and free ligand. The free ligand for **2** was not soluble in the solvent mixture, but the ligand of **4** was soluble in buffer. Consequently when the reduction took place, the free ligand of **2** precipitated from the solution and attenuated the ^{19}F MRI signal. In order to transition into either cellular or animal studies, lower concentrations of probe are desired. To test if lower concentrations could be imaged a 0.5 mM solution of **4** was prepared in PBS and 3 equiv. of cysteine (1.5 mM) were added and then exposed to air. After a 20-minute, a successful image was acquired with an SNR of 13 for the fully reduced sample and when after exposure to air, the SNR decreased to 2. (Figure 10)

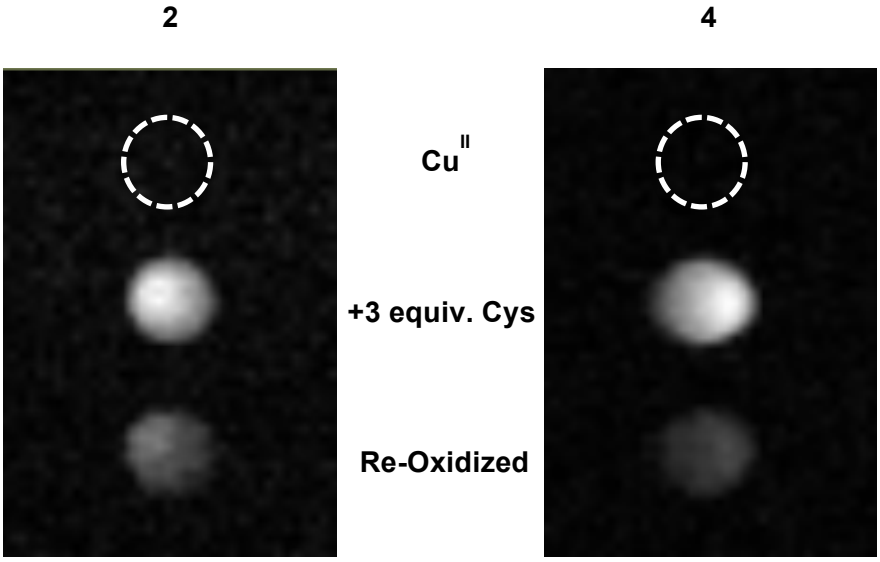

Figure 9. T_1-weighted ^{19}F MRI coronal images at 24 ºC on a 7.0 T MRI scanner. Complex **2** in 50 mM HEPES buffer (pH 7.2) and CH_3CN (6:4, v/v). Complex **4** only in 50 mM HEPES buffer (pH 7.2) Top: 4 mM **2** and **4** in their respective buffer; Middle: 4 mM **2** and **4** with 3 equiv. of cysteine (12mM) Bottom: 4mM **2** and **4** in presence of 12 mM cysteine, re-oxidized for 1 hour. Parameters: T_1-RARE, TE: 14.99 ms, TR:1200 ms, Avg: 256, Rare Factor:16, Image size:64 by 64

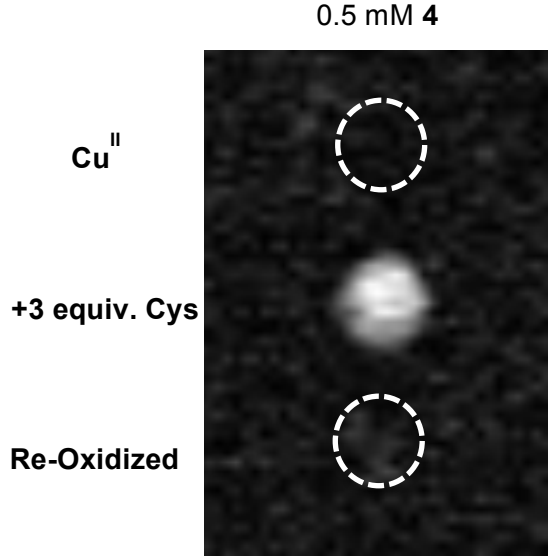

Figure 10. T_1-weighted ^{19}F MRI coronal images at 24 ºC on a 7.0 T MRI scanner. Complex **4** only in PBS buffer (pH 7.4) Top: 0.5 mM **4** ; Middle: 0.5 mM **4** with 3 equiv. of cysteine (1.5 mM of Cysteine) Bottom: 0.5 mM **4** in presence of 1.5 mM cysteine, re-oxidized for 1 hour. Parameters: T_1-RARE, TE: 44.98 ms, TR:1200 ms, Avg: 1024, Rare Factor: 32, Image size:64 by 64

After determining that both **2** and **4** have an efficient reactivity and selectivity toward cysteine, application in a biological system was studied next. Since the solubility of **2** in water was limited, biological studies were carried out with complex **4** since it was soluble up to 1 mM in water. Before these studies were conducted, stability studies in biological pH ranges and with different bio-available metals were performed. In complex **4** there was no change over time in the ^{19}F NMR spectra when it was incubated with 2 equivalents of Ca(II) and Zn(II), These metals were chosen because they are biologically abundant divalent metals. Between pH 5-8 there was no change in the NMR spectra. With pH of 4, there was some evidence of demetallation as a sharp peak emerged at the same chemical shift as the corresponding ligand. With these results, studies with cells that contain high levels of biothiols, such as HeLa[36], were possible. Before incubating complex **4** with cells, the stability of the complex in cell culture media, Dulbecco's Modified Eagle Medium (DMEM), was tested. Complex **4** was dissolved in DMEM at a 0.5 mM concentration and a ^{19}F NMR was acquired. At 0 hours, a sharp peak emerged at -67.5 ppm corresponding to the ligand, after incubating at 37 °C for 24 hours, the peak increased in intensity, hence more demetallation or reduction was occurring. With these results, it was concluded that complex **4** was not suitable for mammalian cancer cells as it was not stable in the cell-culture media DMEM. Cell Studies are on going in red blood cells as these contain a high concentration of biothiols.[37] Like previously, the stability of **4** in the cell medium was tested. Since red blood cells are suspended and stored in phosphate-buffered saline (PBS), complex **4** was dissolved in PBS and incubated at 37 °C. Preliminary results indicate that complex **4** was stable up to 24 hours at 37°C as there was no change in the ^{19}F NMR spectra. Then 0.5 mM of **4** was incubated with 10% RBC for 4 hours at 37 °C and a ^{19}F NMR was acquired. At 0 hours there was no change

in the spectrum, after 4 hours a sharp peak emerged corresponding to the reduced version of **4**. To rule out any side reaction, the red blood cells were treated with 5 mM of N-methylmaleimide, a thiol scavanger, for 30 minutes to inactivate all of the biothiols inside the RBC. Following the inactivation, 0.5 mM of **4** was incubated for 4 hours and a ^{19}F NMR was conducted. The peak corresponding to the reduced version had decreased in intensity, supporting the hypothesis that **4** was being reduced by a bio-thiol inside the RBC.

Conclusion

In summary, here we reported two Cu(II) complexes (**2** and **4**) as potential MRI probes for cysteine. Through incorporation of trifluoromethyl-aryl or fluroroalkyl moieties on the cyclam ligand, appropriate Cu(II/I) redox potentials can be achieved that allow their reactivities towards cysteine. The ^{19}F NMR signals are effectively quenched due to the presence of Cu(II) through paramagnetic relaxation effect (PRE). In solution, the Cu(II) complex reacts rapidly with cysteine and converts to a diamagnetic Cu(I) complex with a single, intense ^{19}F NMR signal which was further demonstrated through ^{19}F MRI. The reduction process can be conveniently reversed through air exposure, which regenerates the Cu(II) complex. Additionally, selectivity towards other amino acids and other thiol or nitrogen containing reductants was observed. Water solubility was important with probes aimed at biological studies and complex **4** exhibits great solubility, up to 1 mM in buffer. Overall, the reversibility and good selectivity of **2** and **4** opens up a different approach for designing cysteine-targeted MRI probes. Further studies including continuing studies with red blood cells are underway to observe cysteine levels in a biological system. Preliminary data involving red blood cells are positive and supports the idea of **4** detecting bioreductants in a biological setting.

III. Materials and Methods

General

All solvents and chemicals were purchased from Sigma-Aldrich, Arkpharm and Fisher Sci. and used as received. The ^{1}H, ^{13}C and ^{19}F NMR spectroscopic measurements were conducted in deuterated solvents from Cambridge Isotope Laboratories (Cambridge, MA), using an AGILENT MR 400 NMR spectrometer at 400, 100, 376 MHz, respectively. The chemical shifts for ^{1}H and ^{13}C NMR were calibrated to the solvent peak, while for ^{19}F NMR were calibrated to 5% TFA in D_2O (δ = -76.55 ppm). Walk-up LC-MS and high-resolution Electrospray Ionization (ESI) mass spectral analyses were performed by the Mass Spectrometry Facility of the Department of Chemistry at UT Austin. Electrochemistry experiments were carried out on a CHI 660D electrochemical workstation from the UT Austin Center for Electrochemistry. X-Ray crystallography was done on an Agilent Technologies SuperNova Dual Source diffractometer using a μ-focus Cu Kα radiation source (λ = 1.5418.) with collimating mirror monochromators. EPR spectra were obtained with a Bruker Biospin EMXplus 114 X-band spectrometer equipped with a liquid nitrogen cryostat. MR images were collected on a Bruker BioSpin (Karlsruhe, Germany) Pharmascan 70/16 magnet with a BioSpec two-channel console and BGA-9s gradient coil in the Imaging Research Center at UT Austin.

Synthesis of 1

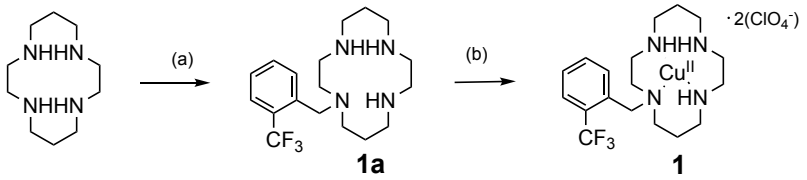

Scheme 1: (a) 1-(bromomethyl)-2-(trifluoromethyl)benzene, K_2CO_3, CH_3CN, 60 ˚C, overnight (60%); (b) $Cu(ClO_4)_2$, MeOH, r.t., overnight (40%)

1-(2-(trifluoromethyl)benzyl)-1,4,8,11-tetraazacyclotetradecane (1a). 1,4,8,11-tetraazacyclotetradecane (Cyclam) (0.228 g, 1.14 mmol) and potassium carbonate (K_2CO_3) (0.525 g, 3.8 mmol) were dissolved under a nitrogen environment with dry CH_3CN (100 mL). 2-(Trifluoromethyl) benzyl bromide (0.1817 g, 0.76 mmol) was dissolved in CH_3CN (25 mL) and was added slowly into the solution. The mixture was refluxed at 60°C for 16 hrs. The mixture was filtered and washed with CH_3CN and concentrated. The product was purified by reverse phase column chromatography (1% CH_3CN in H_2O). (60%) ^{1}H NMR (400 MHz, Chloroform-*d*) δ 7.69 (s, 0H), 7.48 (d, *J* = 4.7 Hz, 1H), 6.73 – 6.62 (m, 5H), 6.62 (d, *J* = 14.2 Hz, 1H), 6.58 (s, 1H), 6.45 (t, *J* = 6.5 Hz, 1H), 2.82 (d, *J* = 4.6 Hz, 1H), 2.39 (d, *J* = 4.8 Hz, 2H), 2.23 – 2.16 (m, 1H), 2.13 (d, *J* = 6.2 Hz, 1H), 2.02 – 1.92 (m, 4H), 1.84 (d, *J* = 15.6 Hz, 3H), 1.02 – 0.89 (m, 3H). ^{19}F NMR (376 MHz, Chloroform-*d*) δ -59.06. HRMS (ESI$^+$): *m/z* 359.2423 [M]+ calcd [C18H29F3N4]+ 359.4612.

[Cu-CyclamBnF3]$(ClO_4)_2$ (1). Compound 1a (0.100 g, 0.279 mmol) and Cu(ClO4)2·6H2O (0.103 g, 0.279 mmol) were dissolved in 3 mL of MeOH and was left stirring overnight at room temperature. A purple precipitate formed after 16hrs, then the solid was centrifuged down and the liquid was decanted. The solid was washed with ethyl ether three times and dried, leaving a light purple solid. (40%) HRMS (ESI$^+$): *m/z*

420.1565 [M]+ calcd [CuC18H28F3N4]+ 420.1562; *m/z* 210.5821 [M]2+ calcd [CuC18H28F3N4]2+ 210.5781.

Synthesis of 2

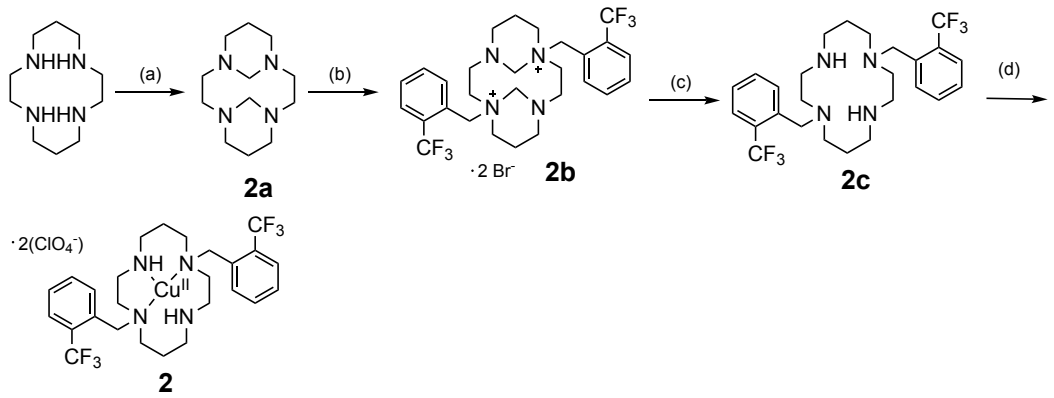

Scheme 2: (a) Formaldehyde (37%wt.), H_2O, 0 ˚C, 2 h (90%); (b) 1-(bromomethyl)-2-(trifluoromethyl)benzene, CH_3CN, r.t., 2 d (30%); (c) NaOH, r.t., 2 d (70%); (d) $Cu(ClO_4)_2$, MeOH, r.t., overnight (80%)

Cyclam bisformyl (2a) was synthesized using literature procedure.[38]

1,8-bis(2-(trifluoromethyl)benzyl)-1,4,8,11-tetraazacyclotetradecane (2c). Cyclam bisformyl (0.150 g, 0.668 mmol) was dissolved in minimal amount of dry CH_3CN (3mL). Then 2-(Trifluoromethyl) benzyl bromide (0.4 g, 1.67 mmol) was added slowly to the solution. The mixture was stirred for 2 days at room temperature. After two days a precipitate formed and was centrifuged down and the liquid was decanted. The solid was washed with minimal amount of CH_3CN and dried, without further purification the compound (2b) was used. Compound 2b (0.120 g, 0.221 mmol) was dissolved in 3M NaOH (15 mL) and 1,4 Dioxane (5mL). The solution was stirred at room temperature for 24 hrs. After 24 hrs the product was extracted with $CHCl_3$ (5X). The organic layer was dried with sodium sulfate and concentrated to obtain a white powder. (70%) ^{1}H NMR (400 MHz, Chloroform-*d*) δ 7.79 (d, *J* = 7.8 Hz, 1H), 7.55 (dd, *J* = 7.9, 1.3 Hz, 1H), 7.38

(t, *J* = 7.6 Hz, 1H), 7.21 (t, *J* = 7.6 Hz, 1H), 3.70 (d, *J* = 1.7 Hz, 2H), 2.82 – 2.68 (m, 4H), 2.68 – 2.56 (m, 4H), 1.81 (p, *J* = 5.6 Hz, 2H). ^{13}C NMR (101 MHz, Chloroform-*d*) δ 138.51, 131.56, 129.57, 126.43, 125.59, 125.53, 123.10, 67.07, 54.29, 51.65, 48.06, 47.73, 26.11. ^{19}F NMR (376 MHz, Chloroform-*d*) δ -59.50. HRMS (ESI$^+$): *m/z* 517.2759 [M]+ calcd [C26H34F6N4]+ 517.2768.

[Cu-CyclamBnF6-trans](ClO$_4$)$_2$ (2). Compound 2b (0.0716 g, 0.139 mmol) and Cu(ClO4)2·6H2O (0.051 g, 0.139 mmol) were dissolved in 3 mL of MeOH and was left stirring overnight at room temperature. A purple precipitate formed after 16hrs and the solid was centrifuged down and the liquid was decanted. The solid was washed with ethyl ether three times and dried giving a dark purple solid. (50%) HRMS (ESI$^+$): *m/z* 578.1898 [M]+ calcd [CuC26H33F6N4]+ 578.1904; *m/z* 289.6000 [M]2+ calcd [CuC26H33F6N4]2+ 289.0952.

Synthesis for 3

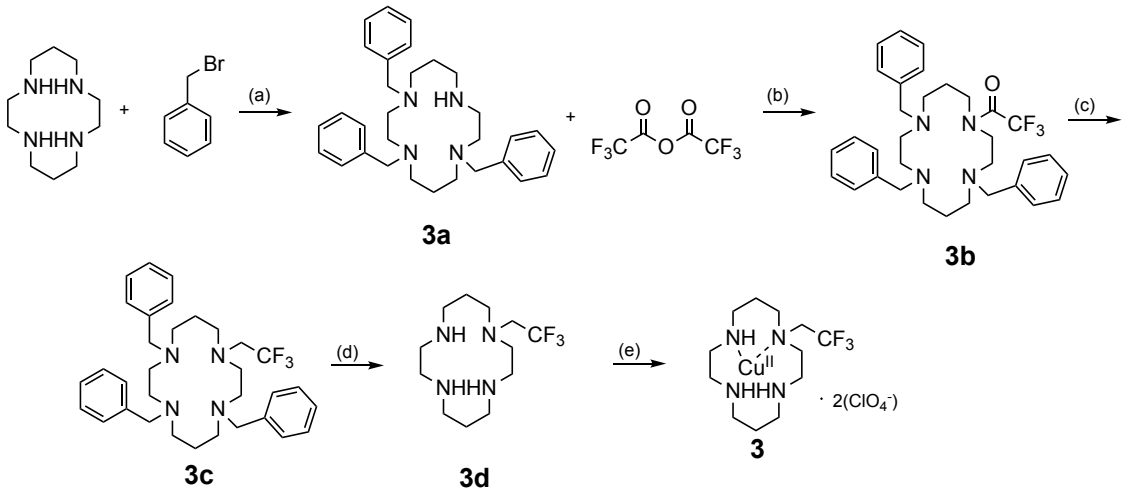

Scheme 3: (a) CH_3CN, r.t., 24h (40%); (b) Et_3N, $CHCl_3$, r.t., 3h (50%); (c) $NaBH_4$, BF_3*Et_2O, Diglyme, 120°C, overnight (90%); (d) 10% Pd/C, H_2, AcOH, r.t., 2d (95%); (e) $Cu(ClO_4)_2$, MeOH, r.t, overnight (40%)

1,4,8-tribenzyl-1,4,8,11-tetraazacyclotetradecane (3a) 1,4,8,11-tetraazacyclotetradecane (Cyclam) (0.100 g, 0.499 mmol) was dissolved in 40 mL of methylene chloride and 2.7 equiv. of benzyl bromide (0.256 g, 1.5 mmol) was added. The solution was stirred for 2 days at room temperature. The solvent was evaporated and purified by reverse phase column chromatography (50% CH_3CN in H_2O) (40%) ^1H NMR (400 MHz, Chloroform-*d*) δ 10.63 (s, 4H), 8.48 (s, 2H), 7.38 – 7.20 (m, 15H), 3.76 (s, 2H), 3.64 (d, *J* = 15.4 Hz, 2H), 3.51 (s, 2H), 3.11 (t, *J* = 5.1 Hz, 2H), 3.00 (s, 2H), 2.84 (s, 2H), 2.78 (d, *J* = 16.4 Hz, 0H), 2.58 (s, 2H), 2.55 – 2.46 (m, 6H), 2.32 (t, *J* = 5.2 Hz, 2H), 1.92 (p, *J* = 6.0 Hz, 4H).

2,2,2-trifluoro-1-(4,8,11-tribenzyl-1,4,8,11-tetraazacyclotetradecan-1-yl)ethan-1-one (3b) Tri-substituted cyclam (3a) (0.055 g, 0.116 mmol) was dissolved in chloroform, then triethylamine (0.0295 g, 0.292 mmol) and trifluoroacetic anhydride (0.049 g, 0.234 mmol) were added. The reaction mixture was stirred at room temperature for 3 hours. The solvent was evaporated and purified by reverse phase column chromatography (50% CH_3CN in H_2O) (50%) ^1H NMR (400 MHz, Chloroform-*d*) δ 7.28 (dq, *J* = 15.2, 7.4 Hz, 15H), 3.67 (s, 2H), 3.58 – 3.38 (m, 6H), 2.69 (s, 6H), 2.60 (q, *J* = 12.4, 9.3 Hz, 4H), 2.40 (t, *J* = 5.8 Hz, 2H), 2.17 (s, 2H), 1.85 (s, 2H). ^{19}F NMR (376 MHz, Chloroform-*d*) δ -69.22 (d, *J* = 20.9 Hz), -75.62.

1,4,8-tribenzyl-11-(2,2,2-trifluoroethyl)-1,4,8,11-tetraazacyclotetradecane (3c) Compound 3b (0.106 g, 0.188 mmol) and sodium borohyrdide (0.035 g, 0.940 mmol) were dissolved in diglyme and stirred. BF_3*Et_2O (0.133 g, 0.94 mmol) was diluted in diglyme and added dropwise into the stirring solution, while the escaping gas (B_2H_6) was passed through a solution of H_2O_2/H_2O/NaOH. Then the solution was heated up to 120°C and stirred overnight. Afterwards, the solution was cooled to room temperature

and 5% sulfuric acid was added dropwise and the volatiles were evaporated in *vacou*. The residue was dissolved with 5% NaOH and the product was extracted with $CHCl_3$ (5x). The organic layers were combined and dried with sodium sulfate, filtered and evaporated. (80%) ^{1}H NMR (400 MHz, Chloroform-*d*) δ 7.42 – 7.17 (m, 15H), 3.51 (s, 2H), 3.45 (d, *J* = 7.4 Hz, 4H), 2.95 (q, *J* = 9.6 Hz, 2H), 2.80 (t, *J* = 6.3 Hz, 2H), 2.74 (t, *J* = 7.1 Hz, 2H), 2.63 – 2.52 (m, 6H), 2.50 (td, *J* = 7.0, 2.7 Hz, 4H), 1.78 – 1.65 (m, 4H). ^{19}F NMR (376 MHz, Chloroform-*d*) δ -69.48 (t, 3F).

1-(2,2,2-trifluoroethyl)-1,4,8,11-tetraazacyclotetradecane (3d) Compound 3c (0.100 g, 0.181 mmol) was dissolved in glacial acetic acid and 10% Pd/C (0.015 g) catalyst was added under N_2. The system was evacuated and filled with H_2. The solution was stirred at room temperature for 2 days. After 2 days the mixture was filtered with celite to remove all of the catalyst and the filtrate was concentrated to received the final product. (90%) ^{1}H NMR (400 MHz, Chloroform-*d*) δ 3.09 (qd, *J* = 18.4, 16.4, 6.7 Hz, 1H), 2.82 – 2.63 (m, 7H), 2.63 (d, *J* = 4.9 Hz, 2H), 2.55 – 2.40 (m, 0H), 1.82 – 1.69 (m, 1H), 1.65 (ddd, *J* = 26.1, 11.6, 5.9 Hz, 1H), 1.28 (s, 1H), 1.23 (s, 12H), 1.19 (s, 3H), 1.06 (d, *J* = 18.2 Hz, 1H), 0.90 – 0.76 (m, 4H), 0.71 (dt, *J* = 14.9, 7.6 Hz, 1H). ^{19}F NMR (376 MHz, Chloroform-*d*) δ -67.14 (t, 3F)

[Cu-CyclamCF$_3$](ClO$_4$)$_2$ (3) Compound 3d (0.0716 g, 0.139 mmol) and Cu(ClO4)2·6H2O (0.051 g, 0.139 mmol) were dissolved in 3 mL of MeOH and was left stirring overnight at room temperature. The solvent was concentrated and purified by reverse phase column chromatography (1% CH_3CN in H_2O) (40%) HRMS (ESI$^+$): *m/z* 344.123 [M]+ calcd [CuC26H33F6N4]+ 344.124;

Synthesis for 4

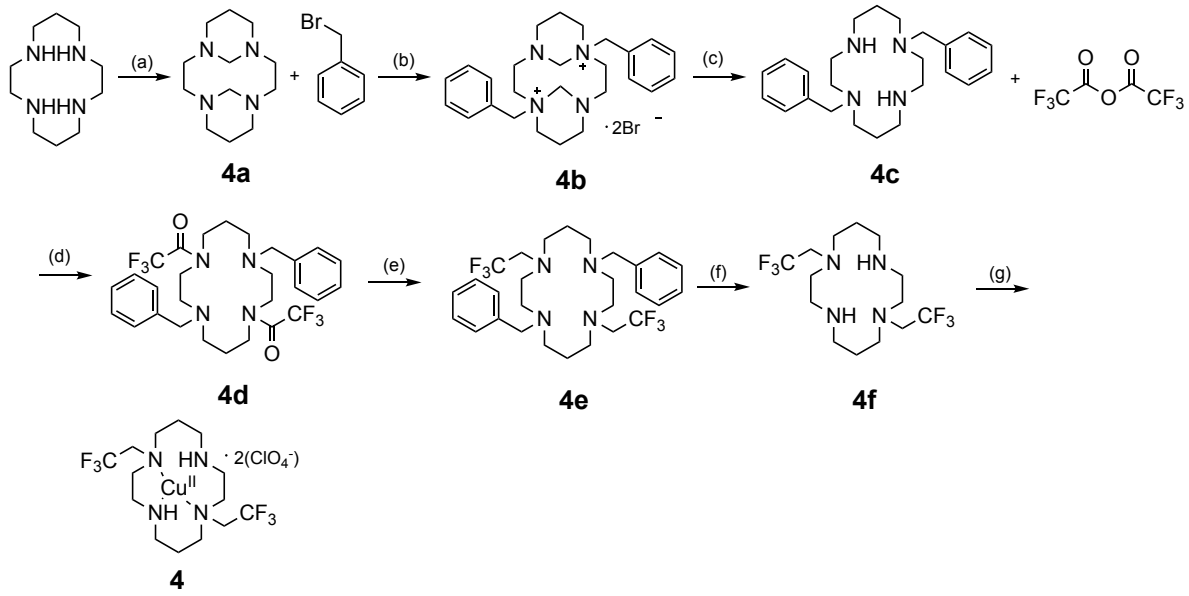

Scheme 4: (a) Formaldehyde (37%wt.) H_2O, 0°C-r.t., 3h (70%); (b) CH_3CN, r.t., overnight (90%); (c) 3M NaOH, r.t., overnight (80%); (d) Et_3N, CH_3Cl, r.t., 3h (60%); (e) $NaBH_4$, $BF_3{*}Et_2O$, Diglyme, 120°C, overnight (60%); (f) 10% Pd/C, H_2, AcOH, r.t., 2d (80%); (g) $Cu(ClO_4)_2$, MeOH, r.t., overnight (80%)

1,8-dibenzyl-1,4,8,11-tetraazacyclotetradecane (4c) was synthesized using literature procedure.[25]

1,8-bis(2,2,2-trifluoroethyl)-1,4,8,11-tetraazacyclotetradecane (4f) was synthesized using a literature procedure.[19]

[Cu-CyclamCF$_6$](ClO$_4$)$_2$ (4). Compound 4f (0.0606 g, 0.166 mmol) and Cu(ClO4)2·6H2O (0.0615 g, 0.166mmol) were dissolved in 5 mL of MeOH and was left stirring overnight at room temperature. A purple precipitate formed and was centrifuged down and the liquid was decanted. The solid was washed with ethyl ether three times and dried giving a dark purple solid. (80%) HRMS (ESI$^+$): *m/z* 427.1358 [M]+ calcd [CuC18H28F3N4]+ 427.1280

Synthesis for control **5**

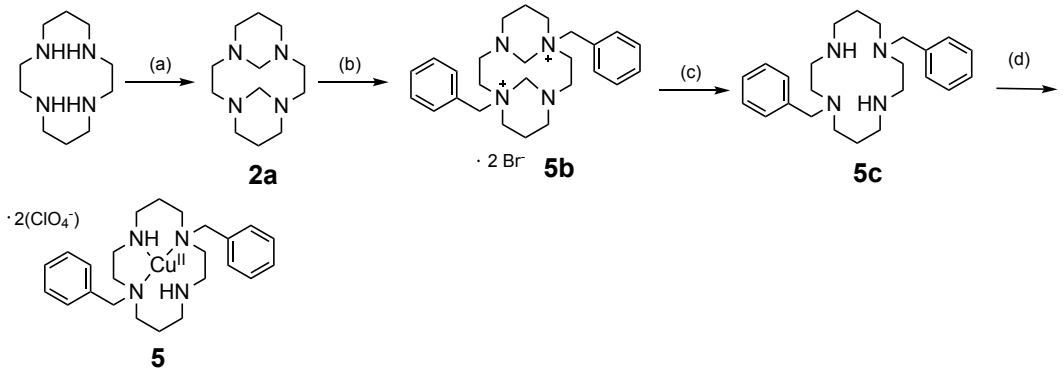

Scheme 5: (a) Formaldehyde (37%wt.), H_2O, 0 ˚C, 2 h (90%); (b) 1-(bromomethyl) benzene, CH_3CN, r.t., 2 d (70%); (c) NaOH, r.t., 2 d (80%); (d) $Cu(ClO_4)_2$, MeOH, r.t., overnight (80%)

Cyclam bisformyl (2a) was synthesized using literature procedure.[25]

1,8-dibenzyl-1,4,8,11-tetraazacyclotetradecane (5c) Cyclam bisformyl (0.100 g, 0.446 mmol) was dissolved in minimal amount of dry CH_3CN (3mL). Then benzyl bromide 0.167 g, 0.98 mmol) was added slowly to the solution. The mixture was stirred for 1 day at room temperature. After a day, a precipitate formed and was centrifuged down and the liquid was decanted. The solid was washed with minimal amount of CH_3CN and dried, without further purification the compound (5b) was used. Compound 5b (0.210 g, 0.535 mmol) was dissolved in 3M NaOH (15 mL) and 1,4 Dioxane (5mL). The solution was stirred at room temperature for 24 hrs. After 24 hrs the product was extracted with $CHCl_3$ (5X). The organic layer was dried with sodium sulfate and concentrated to obtain a white powder. (80%) ^{1}H NMR (400 MHz, Chloroform-*d*) δ 7.27 – 7.07 (m, 10H), 3.63 (s, 4H), 2.73 (s, 3H), 2.62 (dt, *J* = 13.4, 5.3 Hz, 8H), 2.52 – 2.39 (m, 8H), 1.75 (q, *J* = 6.0, 5.4 Hz, 4H)

[Cu-CyclamBn$_2$](ClO$_4$)$_2$ (5) Compound 6c (0.050 g, 0.131 mmol) and Cu(ClO4)2·6H2O (0.048 g, 0.131 mmol) were dissolved in 3 mL of MeOH and was left

stirring overnight at room temperature. A purple precipitate formed after 16hrs and the solid was centrifuged down and the liquid was decanted. The solid was washed with ethyl ether three times and dried giving a dark purple solid. (80%) LRMS (ESI^+): *m/z* 444.1358 [M]+ calcd [CuC24H35N4]+ 444.1280

Synthesis for control **6**

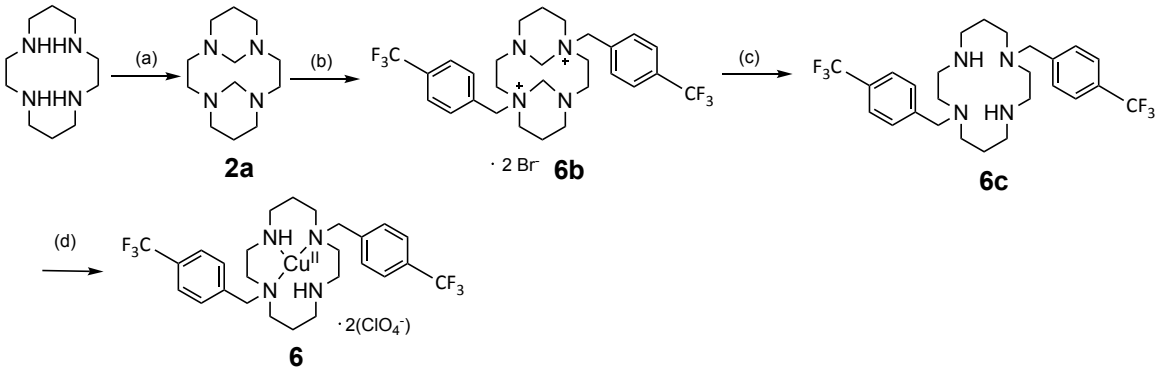

2a **6b** **6c** **6**

Scheme 6: (a) Formaldehyde (37%wt.), H_2O, 0 ˚C, 2 h (90%); (b) 1-(bromomethyl)-4-(trifluoromethyl)benzene, CH_3CN, r.t., 2 d (50%); (c) NaOH, r.t., 2 d (70%); (d) $Cu(ClO_4)_2$, MeOH, r.t., overnight (80%)

Cyclam bisformyl (2a) was synthesized using literature procedure.[25]

1,8-bis(4-(trifluoromethyl)benzyl)-1,4,8,11-tetraazacyclotetradecane (6c)

Cyclam bisformyl (0.080 g, 0.357 mmol) was dissolved in minimal amount of dry CH_3CN (3mL). Then 4-(Trifluoromethyl) benzyl bromide (0.222 g, 0.927 mmol) was added slowly to the solution. The mixture was stirred for 2 days at room temperature. After two days a precipitate formed and was centrifuged down and the liquid was decanted. The solid was washed with minimal amount of CH_3CN and dried, without further purification the compound (6b) was used. Compound 6b (0.130 g, 0.240 mmol) was dissolved in 3M NaOH (15 mL) and 1,4 Dioxane (5mL). The solution was stirred at room temperature for 24 hrs. After 24 hrs the product was extracted with $CHCl_3$ (5X). The organic layer was

dried with sodium sulfate and concentrated to obtain a white powder. (70%) ^{1}H NMR (400 MHz, Chloroform-*d*) δ 7.53 (d, *J* = 8.0 Hz, 4H), 7.42 (d, *J* = 7.9 Hz, 4H), 3.73 (s, 4H), 2.74 (t, *J* = 5.3 Hz, 8H), 2.62 (s, 4H), 2.58 – 2.45 (m, 4H), 1.86 (s, 4H). ^{19}F NMR (376 MHz, Chloroform-*d*) δ -62.23 – -62.52 (t).

[Cu-CyclamBnF6-*p*-trans](ClO$_4$)$_2$ (6) Compound 6c (0.030 g, 0.058 mmol) and Cu(ClO4)2·6H2O (0.022 g, 0.058 mmol) were dissolved in 3 mL of MeOH and was left stirring overnight at room temperature. A purple precipitate formed after 16 hrs and the solid was centrifuged down and the liquid was decanted. The solid was washed with ethyl ether three times and dried giving a dark purple solid. (80%) LRMS (ESI^{+}): *m/z* 578.1898 [M]+ calcd [CuC26H33F6N4]+ 578.1904.

Crystal Structure data

X-ray Experimental for **1**, **2**, and **4** : Crystals grew as clear, violet prisms by slow evaporation from a mixture of CH_3CN and water. The data for crystal **1** was cut from a larger crystal and had approximate dimensions; 0.22 x 0.21 x 0.14 mm. The data for crystal **2** had approximate dimensions; 0.40 x 0.29 x 0.23 mm. The data for crystal **4** had approximate dimensions; 0.28 x 0.27 x 0.23 mm. The data were collected at -167 °C on a Nonius Kappa CCD diffractometer using a Bruker AXS Apex II detector and a graphite monochromator with MoKa radiation (l = 0.71073Å). Reduced temperatures were maintained by use of an Oxford Cryosystems 600 low-temperature device. A total of 645 frames of data were collected using w-scans with a scan range of 1.1° and a counting time of 95 seconds per frame. Details of crystal data, data collection and structure refinement are listed in Table 1. Data reduction were performed using SAINT V8.27B. 1 The structures were solved by direct methods using Superflip 2 and refined by full-matrix

least-squares on F2 with anisotropic displacement parameters for the non-H atoms using SHELXL-2013. 3 Structure analysis was aided by use of the programs PLATON98 4 and WinGX. 5 The hydrogen atoms bound to carbon atoms were calculated in idealized positions. The hydrogen atoms on N2 was observed in a ΔF map refined with an isotropic displacement parameter.

CuCyclamBnF_3 (**1**) Bond Lengths

Atom	Atom	Length/Å	Atom	Atom	Length/Å
C1	N1	1.501(3)	C13	C18	1.500(4)
C1	C2	1.525(4)	C14	C15	1.379(4)
C2	C3	1.516(4)	C15	C16	1.383(4)
C3	N4	1.488(3)	C16	C17	1.388(4)
C4	N4	1.493(3)	C18	F3	1.342(4)
C4	C5	1.511(4)	C18	F2	1.344(3)
C5	N3	1.490(3)	C18	F1	1.356(4)
C6	N3	1.488(3)	N1	Cu1	2.101(2)
C6	C7	1.515(4)	N2	Cu1	2.015(2)
C7	C8	1.520(4)	N3	Cu1	2.026(2)
C8	N2	1.492(3)	N4	Cu1	2.017(2)
C9	N2	1.480(3)	O1	Cl1	1.4589(19)
C9	C10	1.512(4)	O2	Cl1	1.450(2)
C10	N1	1.491(3)	O3	Cl1	1.435(2)
C11	N1	1.511(3)	O4	Cl1	1.434(2)
C11	C12	1.532(4)	O6	Cl2	1.447(2)
C12	C17	1.399(4)	O5	Cl2	1.456(2)
C12	C13	1.414(4)	O7	Cl2	1.438(2)
C13	C14	1.397(4)	O8	Cl2	1.438(2)

Bond Angles for (**1**)

Atom	Atom	Atom	Angle/˚	Atom	Atom	Atom	Angle/˚
N1	C1	C2	114.3(2)	C10	N1	Cu1	103.02(15)
C3	C2	C1	114.7(2)	C1	N1	Cu1	108.02(16)
N4	C3	C2	113.9(2)	C11	N1	Cu1	111.81(15)
N4	C4	C5	108.9(2)	C9	N2	C8	110.1(2)
N3	C5	C4	107.5(2)	C9	N2	Cu1	106.66(16)
N3	C6	C7	112.1(2)	C8	N2	Cu1	117.03(17)

C6	C7	C8	114.8(2)	C6	N3	C5	111.4(2)
N2	C8	C7	111.5(2)	C6	N3	Cu1	117.81(17)
N2	C9	C10	108.0(2)	C5	N3	Cu1	106.71(16)
N1	C10	C9	110.1(2)	C3	N4	C4	109.1(2)
N1	C11	C12	118.2(2)	C3	N4	Cu1	118.31(17)
C17	C12	C13	116.6(2)	C4	N4	Cu1	107.11(16)
C17	C12	C11	120.3(3)	N2	Cu1	N4	175.42(9)
C13	C12	C11	122.9(2)	N2	Cu1	N3	92.54(9)
C14	C13	C12	120.8(3)	N4	Cu1	N3	86.16(9)
C14	C13	C18	116.1(3)	N2	Cu1	N1	86.71(8)
C12	C13	C18	122.9(2)	N4	Cu1	N1	94.42(9)
C15	C14	C13	120.8(3)	N3	Cu1	N1	177.67(9)
C14	C15	C16	119.5(3)	O4	Cl1	O3	110.26(13)
C15	C16	C17	120.1(3)	O4	Cl1	O2	109.79(13)
C16	C17	C12	122.3(3)	O3	Cl1	O2	109.98(12)
F3	C18	F2	106.4(2)	O4	Cl1	O1	109.01(12)
F3	C18	F1	105.8(2)	O3	Cl1	O1	108.91(12)
F2	C18	F1	105.1(3)	O2	Cl1	O1	108.85(11)
F3	C18	C13	113.5(3)	O8	Cl2	O7	109.84(12)
F2	C18	C13	112.9(2)	O8	Cl2	O6	109.90(13)
F1	C18	C13	112.5(3)	O7	Cl2	O6	109.90(12)
C10	N1	C1	109.4(2)	O8	Cl2	O5	108.74(12)
C10	N1	C11	110.4(2)	O7	Cl2	O5	109.75(12)
C1	N1	C11	113.7(2)	O6	Cl2	O5	108.68(12)

CuCyclamBnF_6 (**2**) bond lengths

Atom	**Atom**	**Length/Å**	**Atom**	**Atom**	**Length/Å**
Cu1	N2[1]	1.9855(11)	C4	C5	1.5259(19)
Cu1	N2	1.9855(11)	C5	N1[1]	1.4920(17)
Cu1	N1	2.1181(12)	C6	C7	1.5316(18)
Cu1	N1[1]	2.1182(12)	C7	C12	1.402(2)
F1	C13	1.3442(16)	C7	C8	1.412(2)
F2	C13	1.3468(17)	C8	C9	1.406(2)
F3	C13	1.3574(16)	C8	C13	1.507(2)
N1	C1	1.4919(16)	C9	C10	1.384(2)
N1	C5[1]	1.4920(17)	C10	C11	1.382(2)
N1	C6	1.5105(16)	C11	C12	1.392(2)
N2	C2	1.4857(17)	Cl1	O4	1.4292(13)
N2	C3	1.4878(17)	Cl1	O3	1.4378(12)
C1	C2	1.513(2)	Cl1	O2	1.4420(11)
C3	C4	1.515(2)	Cl1	O1	1.4514(10)

Bond Angles of (**2**)

Atom	Atom	Atom	Angle/°	Atom	Atom	Atom	Angle/°
N2[1]	Cu1	N2	180.0	C12	C7	C6	117.41(13)
N2[1]	Cu1	N1	93.58(4)	C8	C7	C6	125.77(13)
N2	Cu1	N1	86.42(4)	C9	C8	C7	120.33(14)
N2[1]	Cu1	N1[1]	86.42(4)	C9	C8	C13	115.44(13)
N2	Cu1	N1[1]	93.58(4)	C7	C8	C13	124.23(12)
N1	Cu1	N1[1]	180.0	C10	C9	C8	121.22(14)
C1	N1	C5[1]	108.98(10)	C11	C10	C9	119.26(14)
C1	N1	C6	111.10(10)	C10	C11	C12	119.83(15)
C5[1]	N1	C6	112.61(10)	C11	C12	C7	122.67(14)
C1	N1	Cu1	102.32(8)	F1	C13	F2	105.92(12)
C5[1]	N1	Cu1	110.51(8)	F1	C13	F3	105.28(11)
C6	N1	Cu1	110.84(8)	F2	C13	F3	105.84(11)
C2	N2	C3	109.61(11)	F1	C13	C8	112.84(12)
C2	N2	Cu1	108.86(8)	F2	C13	C8	114.31(12)
C3	N2	Cu1	117.05(8)	F3	C13	C8	111.95(12)
N1	C1	C2	109.56(10)	O4	Cl1	O3	110.87(9)
N2	C2	C1	108.69(11)	O4	Cl1	O2	109.97(8)
N2	C3	C4	112.86(11)	O3	Cl1	O2	109.18(7)
C3	C4	C5	114.52(11)	O4	Cl1	O1	108.84(7)
N1[1]	C5	C4	114.64(11)	O3	Cl1	O1	109.07(7)
N1	C6	C7	117.07(10)	O2	Cl1	O1	108.88(7)
C12	C7	C8	116.65(12)				

CuCyclamCF_6 (**4**) bond lengths

Atom	Atom	Length/Å	Atom	Atom	Length/Å
Cu1	N1	2.121(2)	N2	C3	1.489(4)
Cu1	N1[1]	2.121(2)	N2	C7	1.475(4)
Cu1	N2[1]	1.985(3)	C1	C2	1.510(5)
Cu1	N2	1.985(3)	C3	C4	1.496(5)
F1	C1	1.311(5)	C5	C6	1.510(6)
F2	C1	1.318(5)	C6	C7[1]	1.510(5)
F3	C1	1.316(5)	Cl1	O1	1.403(4)
N1	C2	1.477(4)	Cl1	O2	1.420(3)
N1	C4	1.499(4)	Cl1	O3	1.431(3)
N1	C5	1.493(5)	Cl1	O4	1.417(3)

Bond Angles for (**4**)

Atom	Atom	Atom	Angle/°	Atom	Atom	Atom	Angle/°
N1	Cu1	N1[1]	180.0	F1	C1	C2	114.2(3)
N2[1]	Cu1	N1	92.84(11)	F2	C1	C2	114.3(3)

$N2^1$	Cu1	$N1^1$	87.16(11)	F3	C1	F2	106.3(4)
N2	Cu1	$N1^1$	92.84(11)	F3	C1	C2	109.1(4)
N2	Cu1	N1	87.16(11)	N1	C2	C1	120.3(3)
$N2^1$	Cu1	N2	180.0	N2	C3	C4	109.5(3)
C2	N1	Cu1	108.07(18)	C3	C4	N1	110.4(3)
C2	N1	C4	113.1(3)	N1	C5	C6	114.1(3)
C2	N1	C5	112.8(3)	$C7^1$	C6	C5	115.0(3)
C4	N1	Cu1	101.46(19)	N2	C7	$C6^1$	113.5(3)
C5	N1	Cu1	110.9(2)	O1	Cl1	O2	111.2(2)
C5	N1	C4	110.0(3)	O1	Cl1	O3	110.0(2)
C3	N2	Cu1	108.0(2)	O1	Cl1	O4	109.7(3)
C7	N2	Cu1	118.4(2)	O2	Cl1	O3	109.57(19)
C7	N2	C3	110.6(3)	O4	Cl1	O2	109.2(2)
F1	C1	F2	105.8(4)	O4	Cl1	O3	107.2(2)
F1	C1	F3	106.7(3)				

UV/Vis absorption specstroscopy

Data was collected from an Agilent Technologies Cary 60 UV-Vis at room temperature from 200 – 1000 nm, with a fast acquisition rate. The samples were prepared and transferred to a 3mL screw top quartz cuvette inside an anaerobic chamber, with a septum cap placed on top.

Electron Paramagnetic Resonance (EPR)

EPR spectra collected from Bruker Biospin EMXplus 114 X-band spectrometer equipped with a liquid nitrogen cryostat. The spectra of the samples were collected at room temperature. The samples were prepared in vials inside an anaerobic chmber and then transferred into 2 mm EPR tubes before acquisition.

Electrochemistry data (cyclic voltammetry)

Electrochemistry experiments were carried out on a CHI 660D electrochemical workstation. Cyclic voltammetry (CV) measurements for a 1 mM solution of the

compound were recorded at 100 mV/s in a glovebox. A three-electrode cell was used, including a platinum electrode as working electrode, an Ag/Ag+ non-aqueous electrode as reference electrode (a 10 mM DMF solution of AgNO3 was used as the source of Ag+) and a platinum wire as auxiliary electrode. Bn_4NBF_4 (0.1 M) was used as the electrolyte and the spectra were calibrated by ferrocene.

^{19}F MR imaging

The magnetic resonance imaging experiments were performed on a Bruker BioSpin (Karlsruhe, Germany) Pharmascan 70/16 magnet with a BioSpec two-channel console and BGA-9s gradient coil. The RF coil was a quadrature single resonance tunable T/R coil (Doty Scientific, Inc., Columbia, South Carolina, USA) with a resonant frequency of 282.2 MHz to correspond to 19F at 7.0 T. Each element of the RF coil was tuned and matched with the samples loaded using a Morrwasfrequency sweeper (MorrwasInstruments, Inc. Ottawa, Ontario, Canada) while the complementary element was terminated with the receive chain of the instrument. All prescan adjustments and imaging was performed using product sequences and methods in ParaVision 6.0.1 (Bruker, vide supra).

IV. Nuclear Magnetic Resonance Data

NMR Agilent 400 mHz

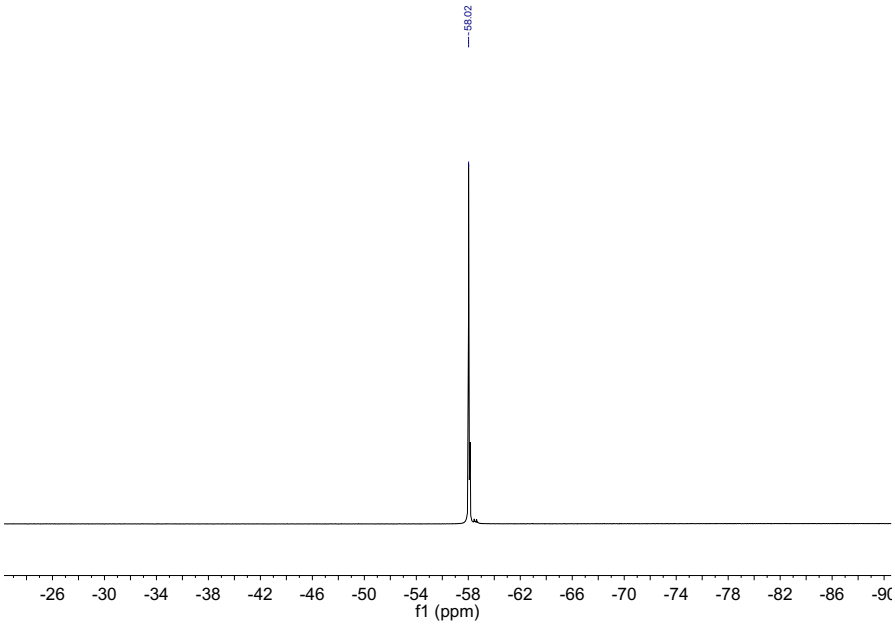

^{19}F NMR spectra of ligand **1a**

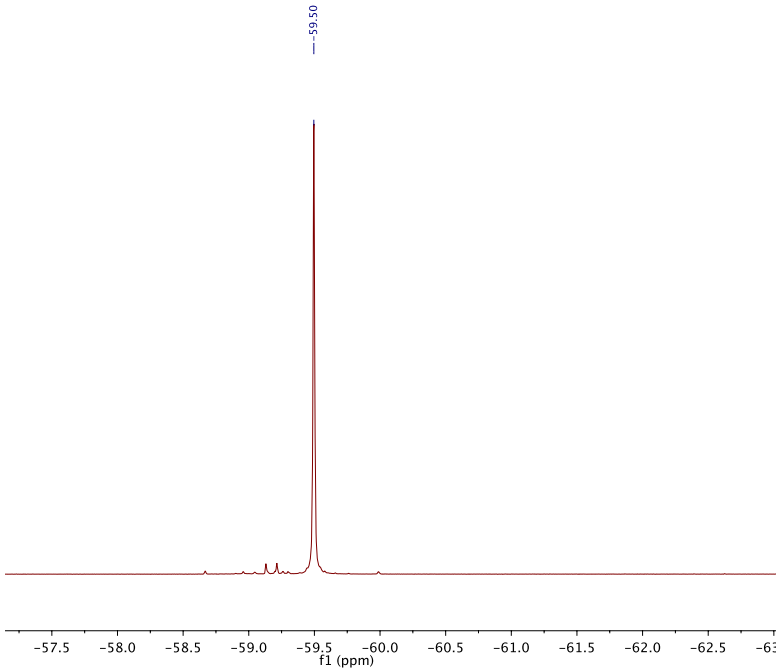

^{19}F NMR of ligand **2c**

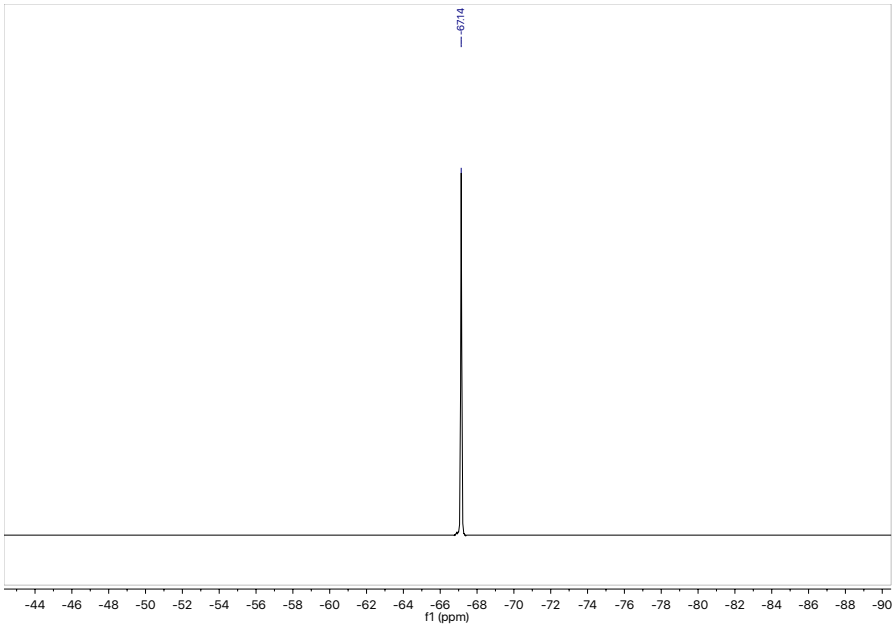

^{19}F NMR spectra of ligand **3d**

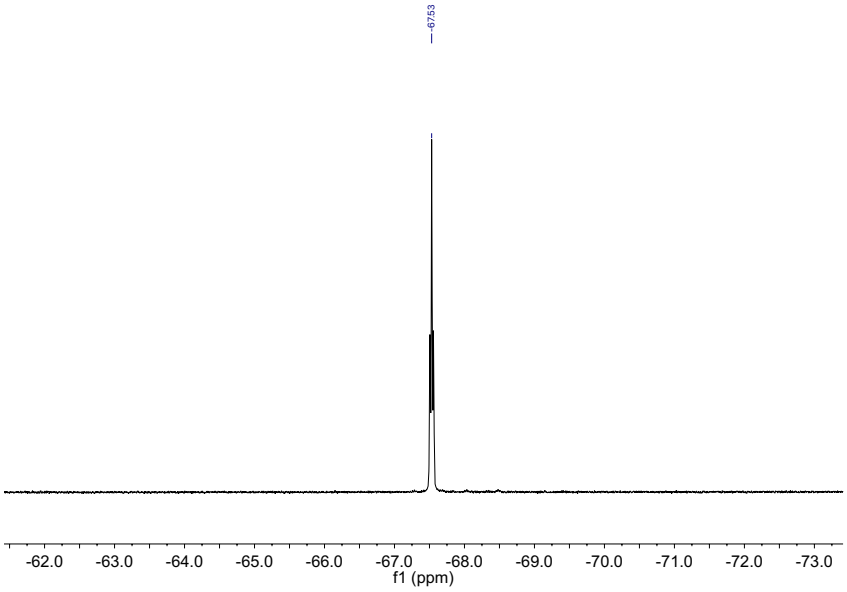

^{19}F NMR spectra of ligand **4f**

V. References:

1. Tian, M.; Guo, F.; Sun, Y.; Zhang, W.; Miao, F.; Liu, Y.; Song, G.; Ho, C. L.; Yu, X.; Sun, J. Z.; Wong, W. Y., A fluorescent probe for intracellular cysteine overcoming the interference by glutathione. *Org Biomol Chem* **2014,** *12* (32), 6128-33.
2. Poole, L. B., The basics of thiols and cysteines in redox biology and chemistry. *Free Radic Biol Med* **2015,** *80*, 148-57.
3. Lu, S. C., Regulation of hepatic glutathione synthesis: current concepts and controversies. *FASEB J* **1999,** *13* (10), 1169-83.
4. Munday, R.; Munday, C. M.; Winterbourn, C. C., Inhibition of copper-catalyzed cysteine oxidation by nanomolar concentrations of iron salts. *Free Radic Biol Med* **2004,** *36* (6), 757-64.
5. Shahrokhian, S., Lead phthalocyanine as a selective carrier for preparation of a cysteine-selective electrode. *Anal Chem* **2001,** *73* (24), 5972-8.
6. Liu, B.; Wang, J.; Zhang, G.; Bai, R.; Pang, Y., Flavone-based ESIPT ratiometric chemodosimeter for detection of cysteine in living cells. *ACS Appl Mater Interfaces* **2014,** *6* (6), 4402-7.
7. Liu, G.; Liu, D.; Han, X.; Sheng, X.; Xu, Z.; Liu, S. H.; Zeng, L.; Yin, J., A hemicyanine-based colorimetric and ratiometric fluorescent probe for selective detection of cysteine and bioimaging in living cell. *Talanta* **2017,** *170*, 406-412.
8. Yang, Z.; Zhao, N.; Sun, Y.; Miao, F.; Liu, Y.; Liu, X.; Zhang, Y.; Ai, W.; Song, G.; Shen, X.; Yu, X.; Sun, J.; Wong, W. Y., Highly selective red- and green-emitting two-photon fluorescent probes for cysteine detection and their bio-imaging in living cells. *Chem Commun (Camb)* **2012,** *48* (28), 3442-4.
9. Li, G.; Chen, Y.; Wu, J.; Ji, L.; Chao, H., Thiol-specific phosphorescent imaging in living cells with an azobis(2,2'-bipyridine)-bridged dinuclear iridium(III) complex. *Chem Commun (Camb)* **2013,** *49* (20), 2040-2.
10. Jung, H. S.; Han, J. H.; Pradhan, T.; Kim, S.; Lee, S. W.; Sessler, J. L.; Kim, T. W.; Kang, C.; Kim, J. S., A cysteine-selective fluorescent probe for the cellular detection of cysteine. *Biomaterials* **2012,** *33* (3), 945-53.
11. Knight, J. C.; Edwards, P. G.; Paisey, S. J., Fluorinated contrast agents for magnetic resonance imaging; a review of recent developments. *RSC Advances* **2011,** *1*, 1415-1425.

12. Tirotta, I.; Dichiarante, V.; Pigliacelli, C.; Cavallo, G.; Terraneo, G.; Bombelli, F. B.; Metrangolo, P.; Resnati, G., (19)F magnetic resonance imaging (MRI): from design of materials to clinical applications. *Chem Rev* **2015,** *115* (2), 1106-29.

13. Liu, G.; Li, Y.; Pagel, M. D., Design and characterization of a new irreversible responsive PARACEST MRI contrast agent that detects nitric oxide. *Magn Reson Med* **2007,** *58* (6), 1249-56.

14. Mizukami, S.; Takikawa, R.; Sugihara, F.; Hori, Y.; Tochio, H.; Wälchli, M.; Shirakawa, M.; Kikuchi, K., Paramagnetic relaxation-based 19f MRI probe to detect protease activity. *J Am Chem Soc* **2008,** *130* (3), 794-5.

15. Mizukami, S.; Takikawa, R.; Sugihara, F.; Shirakawa, M.; Kikuchi, K., Dual-function probe to detect protease activity for fluorescence measurement and 19F MRI. *Angew Chem Int Ed Engl* **2009,** *48* (20), 3641-3.

16. Matsushita, H.; Mizukami, S.; Mori, Y.; Sugihara, F.; Shirakawa, M.; Yoshioka, Y.; Kikuchi, K., 19F MRIMonitoring of Gene Expression in Living Cells through Cell-Surface β-Lactamase Activity. *ChemBioChem* **2012,** *13*, 1579-1583.

17. Nakamura, T.; Matsushita, H.; Sugihara, F.; Yoshioka, Y.; Mizumaki, S.; Kikuchi, K., Activatable ^{19}F MRI Nanoparticle Probes for the Detection of Reducing Environments. *Angew. Chem. Int. Ed.* **2015,** *54*, 1007-1010.

18. Yu, M.; Xie, D.; Phan, K. P.; Enriquez, J. S.; Luci, J. J.; Que, E. L., A Co(II) complex for (19)F MRI-based detection of reactive oxygen species. *Chem Commun (Camb)* **2016,** *52* (96), 13885-13888.

19. Blahut, J.; Bernášek, K.; Gálisová, A.; Herynek, V.; Císařová, I.; Kotek, J.; Lang, J.; Matějková, S.; Hermann, P., Paramagnetic (19)F Relaxation Enhancement in Nickel(II) Complexes of N-Trifluoroethyl Cyclam Derivatives and Cell Labeling for (19)F MRI. *Inorg Chem* **2017,** *56* (21), 13337-13348.

20. Yu, M.; Beyers, R. J.; Gorden, J. D.; Cross, J. N.; Goldsmith, C. R., A magnetic resonance imaging contrast agent capable of detecting hydrogen peroxide. *Inorg Chem* **2012,** *51* (17), 9153-5.

21. Dorazio, S. J.; Morrow, J. R., The Development of Iron(II) Complexes as ParaCEST MRI Contrast Agents. *Eur. J. Inorg. Chem.* **2012**, 2006-2014.

22. Xie, D.; King, T. L.; Banerjee, A.; Kohli, V.; Que, E. L., Exploiting Copper Redox for (19)F Magnetic Resonance-Based Detection of Cellular Hypoxia. *J Am Chem Soc* **2016,** *138* (9), 2937-40.

23. Obata, A.; Yoshimi, E.; Waki, A.; Lewis, J. S.; Oyama, N.; Welch, M. J.; Saji, H.; Yonekura, Y.; Fujibayashi, Y., Retention mechanism of hypoxia selective nuclear imaging/radiotherapeutic agent cu-diacetyl-bis(N4-methylthiosemicarbazone) (Cu-ATSM) in tumor cells. *Ann Nucl Med* **2001,** *15* (6), 499-504.

24. Xie, D.; Kim, S.; Kohli, V.; Banerjee, A.; Yu, M.; Enriquez, J. S.; Luci, J. J.; Que, E. L., Hypoxia-Responsive (19)F MRI Probes with Improved Redox Properties and Biocompatibility. *Inorg Chem* **2017,** *56* (11), 6429-6437.

25. Wadas, T. J.; Wong, E. H.; Weisman, G. R.; Anderson, C. J., Coordinating radiometals of copper, gallium, indium, yttrium, and zirconium for PET and SPECT imaging of disease. *Chem Rev* **2010,** *110* (5), 2858-902.

26. McQuade, L. E.; Lippard, S. J., Fluorescence-based nitric oxide sensing by Cu(II) complexes that can be trapped in living cells. *Inorg Chem* **2010,** *49* (16), 7464-71.

27. Blahut, J.; Hermann, P.; Gálisová, A.; Herynek, V.; Císařová, I.; Tošner, Z.; Kotek, J., Nickel(II) complexes of N-CH2CF3 cyclam derivatives as contrast agents for (19)F magnetic resonance imaging. *Dalton Trans* **2016,** *45* (2), 474-8.

28. Harvey, P.; Kuprov, I.; Parker, D., Lanthanide Complexes as Paramagnetic Probes for 19 F Magnetic Resonance. *Eur. J. Inorg. Chem.* **2012,** *2012* (12), 2015-2022.

29. Goeta, A. E.; Howard, J. A.; Maffeo, D.; Puschmann, H.; Williams, J. A. G.; Yufit, D. S., Copper(II) complexes of the isomeric tetraazamacrocyclic ligands 1,11- and 1,8-bis(2-pyridylmethyl)-1,4,8,11-tetraazacyclotetradecane and of the 1,4,8,11-tetraazacyclotetradecane-5,12-dione analogue at neutral and basic pH. *J. Chem. Soc., Dalton Trans.* **2000,** *0*, 1873-80.

30. Bucher, C.; Duval, E.; Espinosa, E.; Barbe, J.-M.; Verpeaux, J.-N.; Amatore, C.; Guilard, R., First Direct Synthesis of a t*rans*-III Complex of Tetramethylcyclam - Physicochemical Characterization, Electrochemistry and X-ray Crystal Structure of 1,4,8,11-Tetramethyl-1,4,8,11-tetraazacyclotetradecane Copper(II) Bistetrafluoroborate. *Eur. J. Inorg. Chem.* **2001**, 1077-1079.

31. Amatore, C.; Barbe, J.-M.; Bucher, C.; Duval, E.; Guilard, R.; Verpeaux, J.-N., Electron transfer induced topological reorganisations in copper complexes of N-tetrasubstituted tetraazamacrocycles. *Inorganica Chimica Acta* **2003,** *356*, 267-78.

32. Pecci, L.; Montefoschi, G.; Musci, G.; Cavallini, D., Novel findings on the copper catalysed oxidation of cysteine. *Amino Acids* **1997,** *13*, 355-67.

33. Jacoby, C.; Temme, S.; Mayenfels, F.; Benoit, N.; Krafft, M. P.; Schubert, R.; Schrader, J.; Flögel, U., Probing different perfluorocarbons for in vivo inflammation imaging by 19F MRI: image reconstruction, biological half-lives and sensitivity. *NMR Biomed* **2014,** *27* (3), 261-71.

34. Connolly, P. J.; Billo, E. J., 'H NMR Evidence for the R,S,R,S Isomer of the (1,4,8,11-Tetraazacyclotetradecane)nickel(II) Ion. *Inorg. Chem.* **1987,** *26*, 3224-3226.

35. Nakayama, T.; Isobe, T.; Nakamiya, K.; Edmonds, J. S.; Shibata, Y.; Morita, M., Complexes of diphenylarsinic acid and phenylarsonic acid with thiols: a 1H and 13C NMR study. *Magn Reson Chem* **2005,** *43* (7), 543-50.

36. Jiang, X.; Yu, Y.; Chen, J.; Zhao, M.; Chen, H.; Song, X.; Matzuk, A. J.; Carroll, S. L.; Tan, X.; Sizovs, A.; Cheng, N.; Wang, M. C.; Wang, J., Quantitative imaging of glutathione in live cells using a reversible reaction-based ratiometric fluorescent probe. *ACS Chem Biol* **2015,** *10* (3), 864-74.

37. Sabine, J. C., GLUTATHIONE CONCENTRATION AND STABILITY IN THE RED BLOOD CELLS IN VARIOUS DISEASE STATES, AND SOME OBSERVATIONS ON THE MECHANISM OF ACTION OF ACETYL-PHENYLHYDRAZINE. *Br J Haematol* **1964,** *10*, 477-84.

38. Royal, G.; Dahaoui-Gindrey, V.; Dahaoui, S.; Tabard, A.; Guilard, R.; Pullumbi, P.; Lecomte, C., New Synthesis of *trans*-Disubstituted Cyclam Macrocycles - Elucidation of the Disubstitution Mechanism on the Basis of X-ray Data and Molecular Modeling. *Eur. J. Org. Chem.* **1998**, 1971-1975.